Helsinki University of Technology Radio Laboratory Publications
Teknillisen korkeakoulun Radiolaboratorion julkaisuja
Espoo, May 2001 REPORT S 246

# NUMERICAL STUDIES ON A RADIO FREQUENCY HOLOGRAM AND ITS USE IN ANTENNA MEASUREMENTS

**Juha Ala-Laurinaho**

Dissertation for the degree of Doctor of Science in Technology to be presented with due permission for public examination and debate in Auditorium S1 at Helsinki University of Technology (Espoo, Finland) on the 25th of May 2001 at 12 o'clock noon.

**Helsinki University of Technology**
**Department of Electrical and Communications Engineering**
**Radio Laboratory**

**Teknillinen korkeakoulu**
**Sähkö- ja tietoliikennetekniikan osasto**
**Radiolaboratorio**

Distribution:
Helsinki University of Technology
Radio Laboratory
P.O.Box 3000
FIN-02015 HUT
Tel. +358-9-451 2252
Fax. +358-9-451 2152



ISBN 951-22-5446-8
ISSN 1456-3835

Otamedia Oy
Espoo 2001

# Preface

The work for this thesis has been carried out at the Radio Laboratory of the Helsinki University of Technology during 1995–2000.

I wish to thank professor Antti Räisänen for the guidance and support during my research work and for giving me opportunity to work at the Radio Laboratory.

I would like to express my gratitude to Dr. Taavi Hirvonen for his advice and co-operation in the research work. Also, I warmly thank my co-workers at the Radio Laboratory for a good working atmosphere. Especially I want to thank Janne Häkli, Arto Lehto, Petri Piironen, Tomas Sehm, Jussi Säily, and Jussi Tuovinen.

I would like to thank the pre-examiners, professor David Olver and Dr. An Ping Zhao, for their corrections and suggestions for improving this thesis.

This work was financed by Academy of Finland, European Space Agency, National Technology Agency (TEKES), Helsinki University of Technology, and the Graduate school of Electronics, Telecommunications, and Automation (GETA). For my research work, I have received grants from Jenny and Antti Wihuri Foundation, Emil Aaltonen Foundation, Foundation of Technology, and Foundation of the Finnish Society of Electronics Engineers. Their support is warmly appreciated. Also, I would like to acknowledge the Center for Scientific Computing (CSC) for providing their computer resources.

Finally, I thank my wife Arja and sons Riku and Vesa for their support during this thesis work.

Espoo, May 4, 2001

Juha Ala-Laurinaho

# Abstract

This thesis deals with the compact antenna test range (CATR) based on a radio frequency hologram. The emphasis is on the development of the numerical analysis of the hologram. Several holograms have been fabricated and tested assessing the quality of the numerical analysis methods described in this thesis.

A CATR is a potential method for testing the electrically large antennas operating at millimetre and submillimetre wavelengths. These high-gain antennas are needed for remote sensing and radio-astronomical applications. A parabolic reflector is most often used as the collimating element in the CATR. However, at frequencies above 100 GHz, the reflector surface accuracy requirement becomes very stringent. To overcome this problem, it is proposed to use a binary amplitude hologram in the CATR. The hologram is a planar, transmission type of structure and the hologram pattern is realised on the metal plated dielectric film.

Typical requirements for the quiet-zone field quality are maximum amplitude and phase ripples of ±0.5 dB and ±5°, respectively. To achieve these requirements in the iterative hologram design procedure, an accurate method for evaluating the electromagnetic wave transmission through the hologram is needed. In this thesis, the finite difference time domain (FDTD) method is used for calculating the transmission of the hologram. However, the hologram structure is so large (at least several hundreds of wavelengths) that the whole hologram structure cannot be simulated at one time.

Two approaches are used for the simplification of the hologram structure: either 1) only one cut of the hologram is analysed at a time or 2) transmissions of electromagnetic wave through slots of different widths are studied and applied to the whole hologram analysis. The first method is used for optimising the holograms as it gives more accurate results. In addition, it is used when the bandwidth, tolerances, polarisation dependence, and planarity requirements of the hologram CATR are studied. The second method provides a tool for predicting cross-polarisation performance of the hologram CATR.

Experiments have been made at several frequencies: 39, 119, and 310 GHz. The results of these experiments show that the method of analysis developed in this thesis is adequate for designing the holograms. In addition, the feasibility of the hologram CATR operation for antenna measurements is demonstrated.

# Contents

# List of Publications

This thesis is based on the work presented in the following papers:

[P1] T. Hirvonen, J. Ala-Laurinaho, J. Tuovinen, A. V. Räisänen: A compact antenna test range based on a hologram, *IEEE Transactions on Antennas and Propagation*, Vol. 45, No. 8, 1997, pp. 1270–1276.

[P2] J. Ala-Laurinaho, T. Hirvonen, J. Tuovinen, A. V. Räisänen: Numerical modeling of a non-uniform grating with FDTD, *Microwave and Optical Technology Letters*, Vol. 15, No. 3, 1997, pp. 134–139.

[P3] T. Hirvonen, J. Ala-Laurinaho, A. V. Räisänen: Performance analysis of a submillimeter wave hologram CATR, *Proceedings of the 27th European Microwave Conference*, Jerusalem, Israel, September 8–12, 1997, pp. 681–686.

[P4] J. Ala-Laurinaho, T. Hirvonen, A. V. Räisänen: On the planarity errors of the hologram of the CATR, *Proceedings of the IEEE Antennas and Propagation International Symposium*, Orlando, Florida, USA, July 11–16, 1999, pp. 2166–2169.

[P5] J. Ala-Laurinaho, T. Sehm, J. Säily, A. V. Räisänen: Cross-polarization performance of the hologram CATR, *Microwave and Optical Technology Letters*, Vol. 27, No. 4, 2000, pp. 225–229.

[P6] J. Ala-Laurinaho, T. Hirvonen, A. V. Räisänen: A 40 GHz CATR based on a hologram, *Proceedings of the 2nd ESA Workshop on Millimetre Wave Technology and Applications: Antennas, Circuits, and Systems*, Espoo, Finland, May 27–29, 1998, pp. 542–547.

[P7] T. Sehm, J. Ala-Laurinaho, T. Hirvonen, A. V. Räisänen: Antenna measurements using a hologram CATR, *Electronics Letters*, Vol. 35, No. 10, 1999, pp. 757–758.

[P8] J. Ala-Laurinaho, T. Hirvonen, P. Piironen, A. Lehto, J. Tuovinen, A. V. Räisänen, U. Frisk: Measurement of the Odin telescope at 119 GHz with a hologram type CATR, to be published in *IEEE Transactions on Antennas and Propagation*, November 2001.

[P9] J. Säily, J. Ala-Laurinaho, J. Häkli, J. Tuovinen, A. Lehto, A. V. Räisänen: Test results of a 310 GHz Hologram compact antenna test range, *Electronics Letters*, Vol. 36, No. 2, 2000, pp. 111–112.

In addition, this work including contribution by the author is presented also in [1–21]. Professor Antti Räisänen has been supervisor in every paper. All the papers of this content are of joint authorship. A detailed description of contributions of the authors is presented in Chapter 5.

# 1 Introduction

In the near future, there will be several satellite missions for monitoring the atmosphere and outer space at millimetre and submillimetre wavelengths, e.g., mainly Swedish Odin-satellite[1] (119–580 GHz) [22] and missions of the European Space Agency (ESA): FIRST[2] (500–3000 GHz) [23], Planck Surveyor (30–800 GHz) [24], MASTER (200–500 GHz) [25], and SOPRANO (200–500 GHz) [26]. The satellites carry onboard electrically large, high-gain antennas, the measurement of which is a demanding task [27,28].

The most frequently used antenna measurement techniques are the far-field method, the near-field method, and the compact antenna test range (CATR). At the moment, none of these is capable of measuring, e.g., a 1 metre antenna at the frequency of 1 THz. Studies have been made for assessing the feasibility and required development of the measurement techniques for submillimetre wave antenna testing [4,6,7,29–32].

Long distances required for far-field ranges cause too much attenuation and distortion due to the atmosphere. Near-field ranges enable indoor measurements but they are time-consuming and thus requiring very stable measurement equipment. The compact antenna test range allows direct radiation pattern measurement indoors, however, the surface accuracy requirements set for the large reflectors needed are very stringent. Thus, a binary amplitude hologram is proposed for the collimating element in a CATR [33]. The binary amplitude hologram is a planar structure and the hologram pattern is realised on the metal plated dielectric film.

The objective of this thesis is to develop a numerical tool for analysing the radio frequency hologram, and thus to advance the development of the hologram CATR for antenna measurements. An accurate simulation method is needed as the success of the hologram design depends on the quality of the numerical analysis tool. The binary transmission does not predict the actual electromagnetic wave transmission through the hologram sufficiently well. Therefore a method based on two-dimensional FDTD is developed in [P1,P2]. The high-level of accuracy of the analysis is verified with measurements in [P1].

With a good analysis method, properties of the hologram CATR can be studied without time-consuming manufacturing and measurement procedures. The allowable tolerances in the hologram manufacturing and the requirements for the hologram planarity are studied in [P3,P4]. For predicting the cross-polarisation produced by a

[1] Odin was successfully launched on 20th of February, 2001.
[2] FIRST is now known as Herschel Space Observatory.

hologram, an analysis method taking into account the curved slots is developed in [P5].

The feasibility of the hologram CATR for antenna measurements at millimetre and submillimetre wavelengths is demonstrated. A low profile antenna designed for radio links [34] has been measured at 39 GHz. The design and manufacturing of the hologram are presented in [P6]. The measured results are compared with the results of the far-field and near-field scanning measurements in [P7]. The main beam of the Odin telescope has been measured at 119 GHz and the results are reported in [P8]. The operation at submillimetre wavelengths is demonstrated by measuring the quiet-zone field of a CATR, which is based on a 60 cm hologram at 310 GHz in [P9].

This thesis consists of two parts: an overview and nine published papers on the research work. In the overview part, the backgrounds for the research work reported in the included papers are presented. Antenna measurement techniques are presented in Chapter 2. Means for the numerical analysis of the hologram are described in Chapter 3. First, the FDTD method, which is used for calculating the transmission through the hologram, is presented. Then, formulas of the physical optics (PO) are presented. They are used for calculating the radiation of the hologram aperture. The simplifying models for the hologram structure are also depicted in Chapter 3. The generation of binary amplitude holograms and the designing of the holograms for CATR application are presented in Chapter 4. The summary of publications and the contributions of the authors are described in Chapter 5. In conclusions, the most important results of the research work are presented.

# 2 Antenna measurements

## *2.1 Antenna properties*

An antenna is a device that transforms a guided wave into a wave propagating in free space. The antenna is characterised by its properties like radiation pattern, directivity, gain, losses, beam efficiency, and radiation efficiency [35]. The required antenna characteristics depend on the application for which the antenna is used. Antennas are usually reciprocal, which means that their properties are the same whether they are receiving or transmitting. If the antenna is not reciprocal, the antenna has to be measured for the same mode that it is designed to be used for, i.e., for a receiving or a transmitting mode. Figure 2.1 shows the standard spherical coordinate system used in antenna measurements [35]. It is typically defined with respect to a mechanical reference on the antenna.

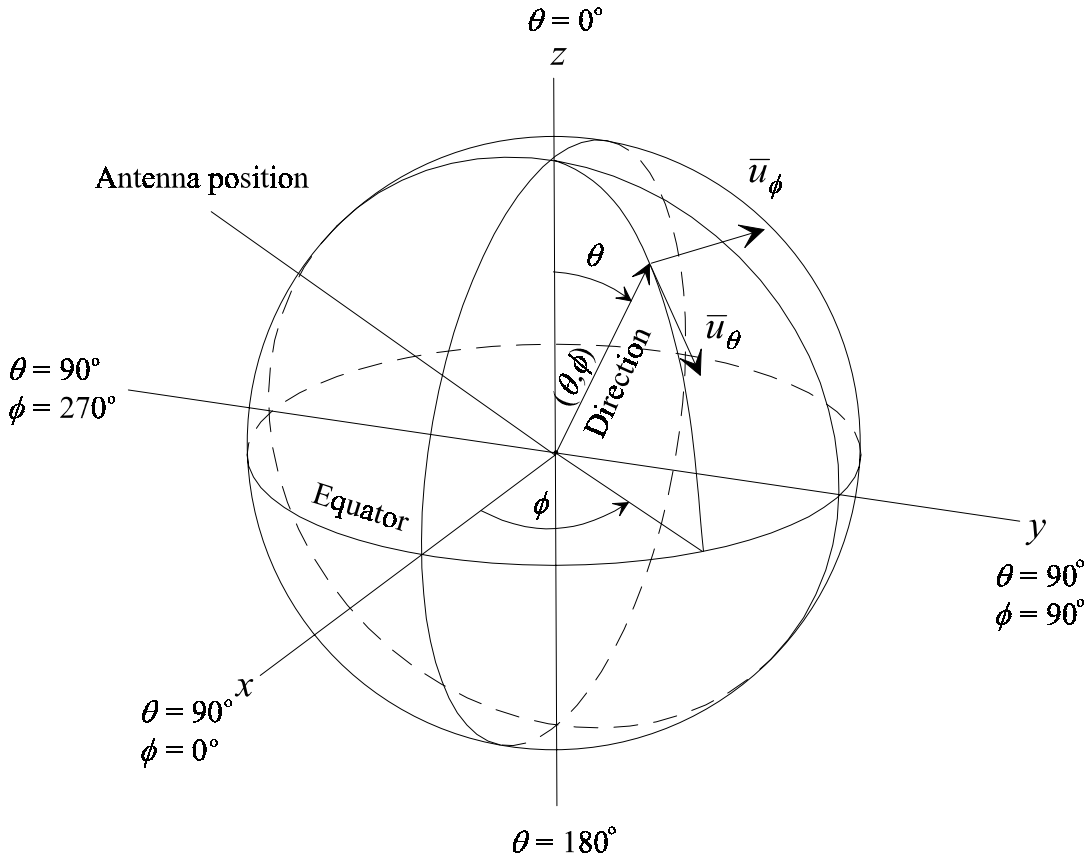


Figure 2.1: Standard spherical coordinate system used in antenna measurements.

Three regions dependent on the distance from the antenna are distinguished [35]: the reactive near-field region, the radiating near-field (Fresnel) region, and the far-field (Fraunhofer) region. The reactive near-field region is in close proximity of the antenna, where reactive fields that decay rapidly with the distance from the antenna

are predominant. The outer boundary for the reactive near-field region depends on the antenna, but usually it is a few wavelengths or less. For an electrically small dipole the reactive field is dominant to about $\lambda/2\pi$, where the reactive and radiating fields are equal.

In the radiating field region, the radiated fields predominate and the region can be divided into the radiating near-field and far-field regions. The former exists for only electrically large antennas while the latter exists for all antennas. In the radiating near-field region the angular field distribution depends on the distance from the antenna, while in the far-field region the angular field distribution is essentially independent on the distance from the antenna. For electrically large, broadside-aperture type of antennas, the boundary between the radiating near-field and the far-field regions is at a distance of $2D^2/\lambda$, where $D$ is the largest dimension of the aperture.

## *2.2 Antenna measurement methods*

An ideal incident field for antenna measurements is a uniform plane wave as most antennas are employed in the far field [36]. In the far-field techniques and compact antenna test ranges, a planar wave front is created while in the near-field techniques the near-field of the test antenna is measured. Numerical methods are required for transforming the near-field data to the far-field characteristics. In addition to these three methods, other methods combining these have been developed [37,38].

### 2.2.1 Far-field ranges

The natural choice for antenna measurements is the far-field method. The separation between the antenna under test (AUT) and the source antenna is so large that the spherical wavefront radiated by the source antenna can be approximated as a plane wave (Figure 2.2). Usually, the allowable phase difference in the AUT aperture area is 22.5° [39]. When the diameter of the AUT is $D$ and the wavelength is $\lambda$, the required separation $d$ between the antennas is $d = 2D^2/\lambda$. For example, at 1 THz the separation has to be larger than 6.7 km for an antenna of 1 m in diameter. Even larger separation than $2D^2/\lambda$ may be needed when very low sidelobe levels are measured [40].

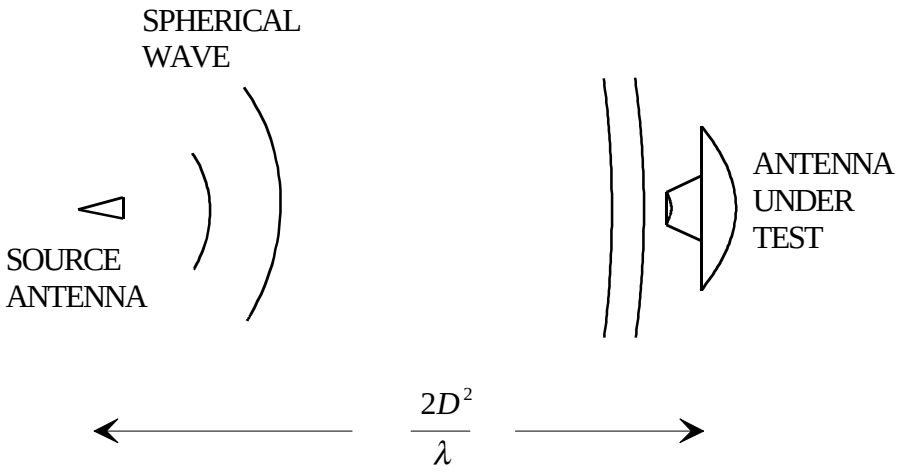


Figure 2.2: Far-field range.

The major problems at millimetre and submillimetre wavelengths are the large attenuation and the distortions to the signal due to the atmosphere. The attenuation caused by resonance of different molecules may be tens of thousands of decibels in one kilometre [28]. This is crucial since the available signal powers at high frequencies are usually very small. Variations of temperature and humidity in time and in space cause distortions to the amplitude and phase of the signal. In practice, the satellites have to be tested indoors where the humidity and temperature can be controlled [28].

The amplitude and phase tapers due to insufficient separation affect the accuracy of the antenna measurement. The too small distance causes widening of the measured main beam, filling of the nulls, and raising of the sidelobe levels [35,41].

### 2.2.2 Near-field ranges

Near-field range measurements can be done indoors in a relatively small space. The temperature and humidity can be controlled and thus the distortions due to the atmosphere become less severe.

First, the amplitude and the phase of the field in a near-by surface of the AUT are sampled with a probe antenna. Then, the far-field radiation pattern of the AUT is calculated using numerical methods, e.g., fast Fourier-transform (FFT). The radiation pattern of the probe antenna is taken into account, when the near-field to far-field transformation is made [42].

The sampling of the near-field can be accomplished over a plane, a sphere, or a cylinder. It is usually practical to measure high-gain reflector antennas with planar or cylindrical scanning [27]. In the planar near-field scanning the AUT is often fixed and

the probe antenna is moved with two linear scanners. There are also other sampling geometries than the rectangular, e.g., plane polar and bi-polar, which require different equipment for moving the probe antenna [42,43]. In the cylindrical scanning the AUT is rotated in one plane and probe is moved with a linear scanner. In the spherical scanning the AUT has to be rotated in two planes. The antennas are often implemented in quite heavy satellites, which makes the accurate rotation of the AUT difficult. Therefore the planar near-field scanning is advantageous.

The sampling area has to be comprehensive so that all the significant energy transmitted by the AUT can be captured [44]. A sampling area that is slightly larger than the aperture of the AUT is sufficient for the planar near-field scanning of high-gain antennas. The size of the sampling area determines the angular range where the measurement results are accurate [45,46].

The sampling has to be dense enough in order to satisfy the Nyquist sampling criterion. The distance between two sampling points has to be smaller than one half of the wavelength [42]. For example, 64 million sampling points are needed for measuring an antenna with diameter of 1 m at 1 THz, when the planar near-field scanning is used. If the sampling rate is 100 samples per second the data acquisition takes about 7 days [29]. Therefore requirements for the stability of the measurement system are very stringent.

The post-processing of the data is however quite fast: for the previous example the fast Fourier-transform and the probe correction take only a few second with an ordinary PC [29]. The required number of the samples and also the complexity of the near-field to far-field transformation depend on the sampling geometry. The post-processing time for the spherical near-field scanning is considerably larger than for the planar or cylindrical near-field scanning [42].

Too coarse sampling causes aliasing of the data resulting in spurious sidelobes, which can partially be avoided by limiting the bandwidth of the Fourier-transform [46]. A coarser sampling grid can be used if only the main beam region and the beam alignment are of interest [42,47].

Other error sources are the phase errors in flexing and bending cables, inaccurate alignment of the probe, and the reflections between the probe and the AUT. Also, the supporting structure of the probe antenna has to be covered carefully with absorbers to prevent reflections [46]. Numerical methods are developed for correction of the phase errors due the cables [48].

The antenna of the NASA SWAS-satellite (Submillimeter Wave Astronomy Satellite) has been successfully tested with the planar near-field scanning at frequencies of 491 GHz and 552 GHz. The aperture size of this offset Cassegrain-type of antenna is 53 cm × 68 cm [47].

### 2.2.3 Compact antenna test ranges

In a compact antenna test range (CATR) the spherical wave front is transformed into a plane wave with a focusing element, which can be a reflector, a lens, or a hologram. Also, an array of antennas may be used to produce a plane wave at low frequencies [41,49]. CATRs enable the antenna measurements indoors in plane wave conditions, i.e., the radiation pattern can be directly measured by rotating the AUT. The main beam of a high-gain antenna can be measured without rotating the AUT by scanning the CATR feed transversally.

The AUT is placed into the quiet-zone that is the extent of the volume where the wave front meets the requirements set on the plane wave. Typically, the maximum amplitude and phase deviations have to be less than ±0.5 dB and ±5°, respectively [4].

#### 2.2.3.1 CATR based on a reflector

The reflector based CATR was invented in the 1960's [50,51]. Today, the reflector ranges are widely used at frequencies below 40 GHz [52], and they have been used for frequencies up to 200 GHz.

Figure 2.3 shows a CATR based on an off-set reflector. The feed horn radiates a spherical wavefront, which reflects from the parabolic reflector forming a plane wave. The diameter of the quiet-zone is limited to one third of the reflector diameter due to the edge diffraction caused by the reflector edges. The illumination in the edges of the reflector has to be low enough to prevent the disturbance of the diffracted fields. The edge diffraction can be diminished by treatment of the reflector edges, e.g., the edge can be rolled or serrated, or the edges can be covered with resistive film [41].

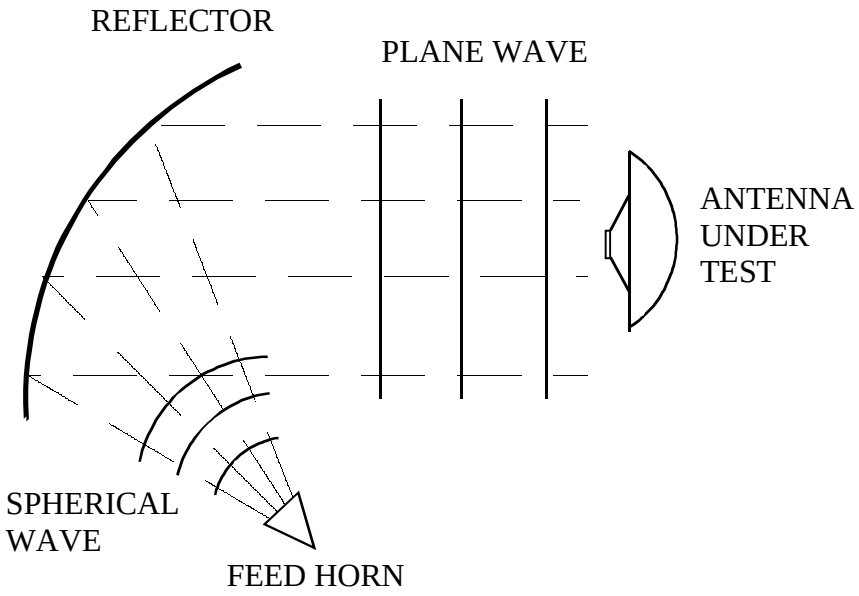


Figure 2.3: An off-set reflector CATR.

With two or more reflectors the quiet-zone size can be substantially increased. Also, the cross-polarisation of the range can be reduced compared to the one reflector range [52]. Using a hyperboloid (Cassegrain system) or an ellipsoid (Gregorian system) subreflector with a paraboloid main reflector the inherent cross-polarisation can be cancelled. The diameter of the quiet-zone can be about 70 % of the main reflector diameter [52].

Another approach is to shape the subreflector so that the amplitude of the illumination of the main reflector is flat in the middle and decreases rapidly towards the edges for preventing the edge diffraction [52]. A planar phase front is achieved by appropriately shaping the main reflector. Thus, two shaped reflectors different from basic shapes of paraboloid, hyperboloid, or ellipsoid, are needed. The problem in the use of two reflectors is that two fairly large and expensive reflectors are needed.

Dual-reflector system of two parabolic cylindrical reflectors offers also better performance with respect to the single-reflector configuration. The advantage of the cylindrical reflectors is that they can be manufactured more easily and thus the manufacturing costs are reduced compared to the doubly curved reflectors [53].

A recently presented configuration is a CATR based on three reflectors (tri-reflector CATR) [54]. With the aid of a dual reflector feed system (DRFS) the illumination of the main reflector can be shaped so that the quiet-zone diameter is about 80 % of the main reflector diameter. The two subreflectors are substantially smaller than the main reflector and therefore the manufacturing of them is less expensive. When the focal

length is large enough the shape of the main reflector can be spherical [4,31]. The manufacturing of an accurate spherical surface is easier than the manufacturing of a paraboloid, thus the manufacturing is less expensive and the accuracy for the main reflector is expected to be sufficient also at terahertz region [31].

The bandwidth of the reflector CATR is fairly large. The minimum operation frequency is determined by the edge diffraction and the maximum frequency is determined by the surface accuracy of the reflectors, assuming, that appropriate feeds are available for each subband. The major problem is the very stringent surface accuracy requirement at high frequencies. Usually the RMS surface error should be less than $0.01\lambda$ [27,35], e.g., 3 μm at 1 THz. This surface error corresponds to a phase error of 7.2 degrees. Good accuracy means large manufacturing costs or even development of new manufacturing techniques.

Large reflectors may have to be made of several pieces. The smaller pieces can be made more accurately, but the alignment and joining of the pieces have to be made carefully. Small gaps often occur between the pieces disconnecting the surface currents and thus deteriorating the performance of the reflector. Tapes are applied to improve the reflector operation [55].

### 2.2.3.2 CATR based on a lens

The idea of using a lens as the collimating element in a CATR was introduced in the end of the 1970's [56,57]. Figure 2.4 shows a CATR based on a dielectric lens. The achievable quiet-zone diameter is about 70–75 % of the lens diameter [56,58].

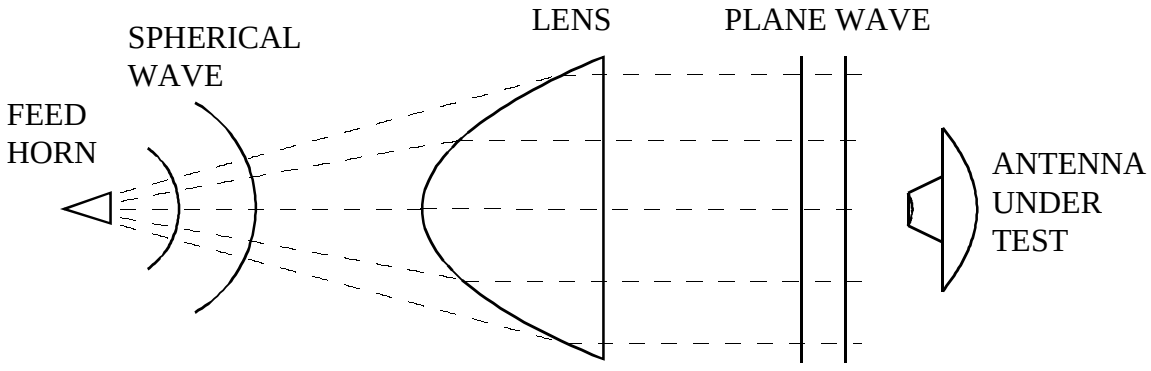


Figure 2.4: Lens type of a CATR.

The surface accuracy requirements for lenses are not as stringent as for reflectors, since the lens is a transmission type of an element. The largest allowable RMS surface

error for a lens is obtained by multiplying that of the reflector by factor $\sqrt{2}/(\sqrt{\varepsilon_r}-1)$ [58].

When the relative permittivity or the dielectric constant $\varepsilon_r$ is less than 1.2, the surface accuracy requirement moderates quickly. On the other hand, the thickness of the lens increases substantially when the dielectric constant decreases. When $\varepsilon_r$ = 1.1 and the ratio between the focal length and the diameter of the lens is $F/D$ = 3, the thickness of the lens is only slightly smaller than the diameter [58]. The dielectric constant affects also the reflection from the lens surface: the larger $\varepsilon_r$ is the more of the power radiated by the feed is reflected from the lens surface.

In practice, the major problem is to find suitable material for lenses [28]. If $\varepsilon_r$ is small, like for foam, the material is usually not homogeneous. The problem is more severe at higher frequencies.

Another problem is the edge diffraction, which, however, has less effect on the performance of the lens CATR than that of the reflector CATR [52]. For minimizing the edge diffraction, serrated metal plates may be used with the lens [58]. The serrated pattern can be manufactured on the metal plated dielectric film or on a plain metal plate. Furthermore, the surfaces of the lens can be shaped in order to achieve an appropriate aperture distribution.

As the CATR based on a reflector operates well at microwave frequencies, the development of the lens type CATR has not been seen very interesting [52]. A demonstrator CATR based on a lens has been made for 110 GHz [58]. Measurements with a 50 cm lens have also been used to help the designing of a 30 cm reflector antenna at 94 GHz [59].

#### 2.2.3.3 CATR based on a hologram

The idea of using computer generated hologram as the collimating element of a CATR was presented in the beginning of the 1990's [33]. It is a potential antenna measurement method especially for millimetre and submillimetre wavelengths. Figure 2.5 shows the principle of the CATR based on a hologram. The hologram modulates the spherical wave radiated by a feed horn in such a way that a plane wave is formed.

The hologram used in the compact antenna test range is a transmission type, binary amplitude hologram [60]. The hologram pattern is made on a metal plated dielectric film. In principle, the hologram pattern can be calculated numerically when the incident and outgoing wave fronts are known [61]. The slots of the hologram are

tapered near the edges of the hologram in order to reduce the edge diffraction. Figure 2.6 shows an example of a binary amplitude hologram. Black parts block the wave and the white parts let the wave propagate through the structure.

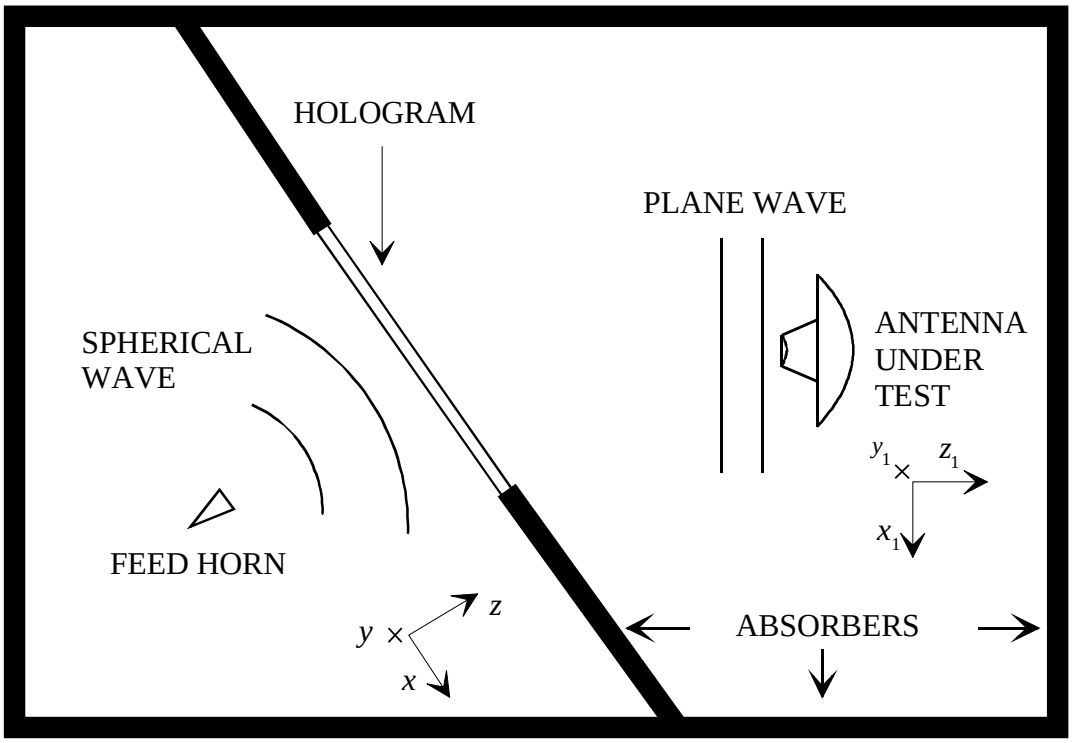


Figure 2.5: Hologram type of a CATR.

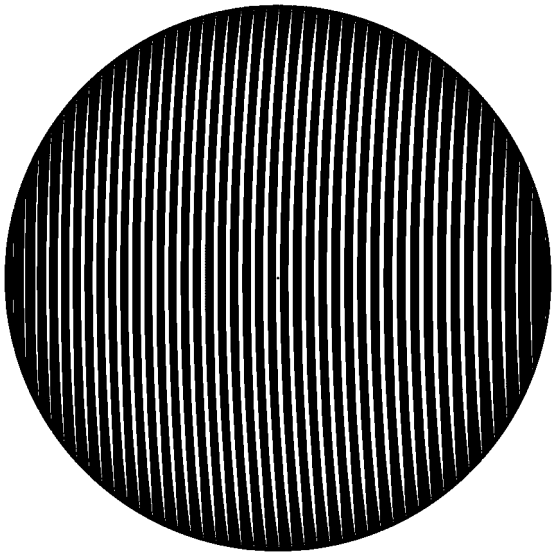

Figure 2.6: Example of a binary amplitude hologram.

The hologram is designed in such a way that the plane wave leaves the hologram in an angle of 33 degrees with respect to the hologram normal. Thus, the diffraction modes, which are propagating to the hologram normal direction, do not disturb the quiet-zone field [60].

The major difference between the radio frequency hologram and other collimating elements is that significant portion of the energy reflects backwards from the hologram. Also, all of the transmitted energy does not propagate to the direction of 33°. Therefore, a powerful signal source is needed, especially, when the quality of the quiet-zone field is checked. In actual measurements of high-gain antennas, the achievable power affects the dynamic range of the measurements. With the same instrumentation, the achievable dynamic range is smaller in the case of the hologram than that in the case of other collimating elements such as a reflector or lens.

The surface accuracy requirement of the hologram is considerably less stringent than that of a reflector [P3]. The hologram is stretched into a frame, which ensures sufficient planarity for the hologram. According to the simulations, the accuracy requirement for the hologram pattern is about $0.01–0.02\lambda$, which is of the same order as the surface accuracy for the reflector. However, the manufacturing of the two-dimensional hologram is easier than the manufacturing of the three-dimensional reflector surface, thus the manufacturing costs are reduced substantially.

The accuracy of the current manufacturing technologies (i.e., wet etching, exposure through a mask) enables the hologram manufacturing up to about 500 GHz, if the size of the hologram is not very large (dimensions less than 600 mm). A theoretical tolerance analysis carried out for a small (200 mm in diameter) hologram at 500 GHz is presented in [P4,6,8]. A theoretical tolerance analysis based on the binary transmittance is presented in [62].

The relation between the hologram and the quiet-zone sizes depends on the required size of the quiet-zone and frequency. In practice, the proportional area, where the tapering of the slots is accomplished, decreases when the size of the hologram increases [P1]. Therefore the ratio of the quiet-zone and hologram sizes is larger for larger holograms. For example, at 119 GHz for the 550 mm hologram the quiet-zone diameter is about 43 % of the hologram diameter, when for the 2.4 m $\times$ 2.0 m hologram the quiet-zone diameter is about 70 % of the smaller dimension [P1,P8].

A CATR based on a reflector or a lens operates well with all polarisations and frequencies (the edge diffraction and the surface accuracy give limitations). However, the operation of a hologram depends fairly strongly on the frequency and polarisation,

because it is a diffractive element. The bandwidth of the hologram CATR is only about ±5–10 % depending on the quiet-zone field requirements.

Due to the polarisation dependency, holograms have to be designed for vertical and horizontal polarisations separately. It is not possible to design a hologram for a polarisation different from these two linear polarisations with the current design method. One possibility to decrease the polarisation dependency maybe the use of subreflectors in the feed of the hologram. By shaping the illumination the edge tapering could be smaller and the widths of the slots over the hologram could be more constant [4,16,21].

The previously used numerical hologram analysis method [33] based on binarized transmission and physical optics (PO) is not accurate enough for predicting the operation of the hologram CATR. The use of the FDTD for calculating the transmission through the hologram and the physical optics for calculating the radiation of the hologram aperture provides a tool for hologram simulation and optimisation [P1,P2,2,3].

### 2.2.4 Other methods

The difficulties in the methods described above have led to the development of other antenna measurement methods. The refocusing of the AUT is used for trying to solve the problem of the large measurement distance in the far-field measurements. In the operation, antennas are usually focused to infinity. In the measurements, however, the AUT is focused to a finite test distance that is significantly smaller than the required far-field distance. It is assumed that the measurement results describe the performance of the AUT also when it is refocused to the infinity. This method applies for antennas, which can be refocused, e.g., electronically phased arrays, or paraboloids and lenses, which can be refocused by axial movement of the feed [63].

Amplitude only measurements are proposed for near field scanning for alleviating the problems of the accurate phase measurements. This leads to a problem of the phase retrieval [64]. In practice, all the phase retrieval methods involve numerical techniques [65].

Holographic methods are proposed for phase retrieving of the near-field measurements. The phase information can be recovered by using a reference antenna or by scanning at two planes or at two cylindrical surfaces [66,67]. A method using a reference antenna and recording of the hologram and thus the phase information is presented in [66]. Methods using two scanning surfaces are described in [65,67,68].

A method using only one planar intensity scan is proposed in [69] for retrieving the phase of the aperture field of the AUT. The method uses Fourier-transform relation between the aperture and scan planes. FFT offers means for iterating the aperture phase rapidly. This method is however restricted for very high-gain antennas and it requires an estimation for the aperture taper. Also, the required scan area is large compared to the AUT.

A hybrid approach to the compact antenna test ranges and the near-field measurements is the single-plane collimating range (SPCR) [37]. The AUT is illuminated with a cylindrical wave front that can be produced by a cylindrical reflector. The vertical crosscut of the reflector has a parabolic curvature and the horizontal crosscut is a line. A one-dimensional numerical algorithm is sufficient to transform the results of the cylindrical wave (near-field) measurements into the desired plane wave (far-field) results. A similar idea for reducing the scan time and simplifying the near-field to far-field transformation is the use of the linear near-field probe in the semi-compact antenna test range (SCATR) [38].

# 3 Numerical analysis of the radio frequency hologram

The numerical analysis of the radio frequency hologram is based on the combination of the finite difference time domain (FDTD) and the physical optics (PO) methods [P2]. The aperture field of the hologram is calculated with the FDTD and the radiation of the aperture is then calculated with the PO. These two methods are described in Sections 3.1 and 3.2. The hologram structure is large in wavelengths and at the same time it contains very fine details compared to the wavelength. The full analysis of the whole hologram structure is impossible and therefore the hologram structure has to be simplified. This has been done in two different ways, which are described in Section 3.3.

## *3.1 FDTD method*

### 3.1.1 Formulation of updating equations

Finite difference time domain method is a versatile method for analysing electromagnetic problems with complex geometries [70,71]. Yee proposed the method first in the 1960's [72]. The derivation of the updating equations for the electric and magnetic field components begins from studying the Maxwell's first and second equations:

$$\nabla \times \overline{E} = -\frac{\partial \overline{B}}{\partial t} + \sigma^* \overline{H}, \tag{3–1}$$

$$\nabla \times \overline{H} = \frac{\partial \overline{D}}{\partial t} + \overline{J}. \tag{3–2}$$

When taking into account the material equations $\overline{D} = \varepsilon \overline{E}$, $\overline{B} = \mu \overline{H}$, and $\overline{J} = \sigma \overline{E}$, equations (3–1) and (3–2) can be written in the component form

$$\frac{\partial E_x}{\partial t} = \frac{1}{\varepsilon}\left(\frac{\partial H_z}{\partial y} - \frac{\partial H_y}{\partial z} - \sigma E_x\right), \tag{3–3}$$

$$\frac{\partial E_y}{\partial t} = \frac{1}{\varepsilon}\left(\frac{\partial H_x}{\partial z} - \frac{\partial H_z}{\partial x} - \sigma E_y\right), \tag{3–4}$$

$$\frac{\partial E_z}{\partial t} = \frac{1}{\varepsilon}\left(\frac{\partial H_y}{\partial x} - \frac{\partial H_x}{\partial y} - \sigma E_z\right), \tag{3–5}$$

$$\frac{\partial H_x}{\partial t} = \frac{1}{\mu}\left(\frac{\partial E_y}{\partial z} - \frac{\partial E_z}{\partial y} - \sigma^* H_x\right), \tag{3–6}$$

$$\frac{\partial H_y}{\partial t} = \frac{1}{\mu}\left(\frac{\partial E_z}{\partial x} - \frac{\partial E_x}{\partial z} - \sigma^* H_y\right), \tag{3–7}$$

$$\frac{\partial H_z}{\partial t} = \frac{1}{\mu}\left(\frac{\partial E_x}{\partial y} - \frac{\partial E_y}{\partial x} - \sigma^* H_z\right). \tag{3–8}$$

An unphysical variable, the magnetic conductance $\sigma^*$, is included in the previous equations. It is necessary when the perfectly matched layer (PML) absorbing boundary condition (ABC) is composed [73]. Central difference approximations are used to discretise the six scalar equations with respect to the time and space:

$$\frac{\partial F(x)}{\partial x}\Big|_{x=x_0} = \frac{F(x_0 + \frac{1}{2}\Delta x) - F(x_0 - \frac{1}{2}\Delta x)}{\Delta x}. \tag{3–9}$$

This central difference approximation leads to the Yee's cell [72], and updating equations for the six scalar field components (three electric and three magnetic) are formed.

FDTD simulation advances in time with discrete time steps. Every second time step electric field components are updated and every second the magnetic field components are updated. It is convenient to calculate the electric and magnetic field components in different points since the updating equation of an electric field component comprises of magnetic field components in neighbouring points and the value of the same electric field component at the previous time step. Correspondingly, the updating equation of a magnetic field comprises of electric field components in neighbouring points and the same magnetic field component at the previous time step.

An electric or a magnetic field component at a discrete point in a uniform lattice and at a discrete time step is denoted as:

$$F^n(q,r,s) = F(q\Delta x, r\Delta y, s\Delta z, n\Delta t). \tag{3–10}$$

For calculating the electric current, the following equation is used:

$$J^{n+\frac{1}{2}}(q,r,s) = \tfrac{1}{2}\sigma\left(E^{n+1}(q,r,s) + E^n(q,r,s)\right). \tag{3–11}$$

For example, the updating equation constituted for the *x*-polarised component of the electric field is

$$E_x^{\,n+1}(q,r,s) = \frac{2\varepsilon - \Delta t\sigma}{2\varepsilon + \Delta t\sigma} E_x^{\,n}(q,r,s) + \frac{2\Delta t}{2\varepsilon + \Delta t\sigma}\left[\frac{1}{\Delta y}(H_z^{\,n+\frac{1}{2}}(q,r+\tfrac{1}{2},s) - H_z^{\,n+\frac{1}{2}}(q,r-\tfrac{1}{2},s)) - \frac{1}{\Delta z}(H_y^{\,n+\frac{1}{2}}(q,r,s+\tfrac{1}{2}) - H_y^{\,n+\frac{1}{2}}(q,r,s-\tfrac{1}{2}))\right]. \quad (3\text{–}12)$$

Generally, the permittivity and conductivity depend on the space, i.e., $\varepsilon = \varepsilon(q,r,s)$ and $\sigma = \sigma(q,r,s)$. In the updating equations of the magnetic field the permeability $\mu = \mu(q,r,s)$ is taken into account [70].

### 3.1.2 Two-dimensional case

The simplified structures used for the analysis of the hologram enable the use of two-dimensional FDTD. The calculation can be carried out separately for two linear polarisations. The set of six scalar equations is reduced into two systems of three equations. For the field components $E_y$, $H_x$, and $H_z$ the system can be written as:

$$\frac{\partial E_y}{\partial t} = \frac{1}{\varepsilon}\left(\frac{\partial H_x}{\partial z} - \frac{\partial H_z}{\partial x} - \sigma E_y\right), \quad (3\text{–}13)$$

$$\frac{\partial H_x}{\partial t} = \frac{1}{\mu}\left(\frac{\partial E_y}{\partial z} - \sigma^* H_x\right), \quad (3\text{–}14)$$

$$\frac{\partial H_z}{\partial t} = \frac{1}{\mu}\left(-\frac{\partial E_y}{\partial x} - \sigma^* H_z\right). \quad (3\text{–}15)$$

Correspondingly, for the field components $E_x$, $E_z$, and $H_y$ the system of three equations is

$$\frac{\partial E_x}{\partial t} = \frac{1}{\varepsilon}\left(-\frac{\partial H_y}{\partial z} - \sigma E_x\right), \quad (3\text{–}16)$$

$$\frac{\partial E_z}{\partial t} = \frac{1}{\varepsilon}\left(\frac{\partial H_y}{\partial x} - \sigma E_z\right), \quad (3\text{–}17)$$

$$\frac{\partial H_y}{\partial t} = \frac{1}{\mu}\left(\frac{\partial E_z}{\partial x} - \frac{\partial E_x}{\partial z} - \sigma^* H_y\right). \quad (3\text{–}18)$$

The hologram is optimised for one linear polarisation (for $E_y$ or $E_x$) at a time, so the separation of two polarisations saves also time in the optimisation process. The separation means also that two-dimensional FDTD does not predict the generation of

the cross-polarisation. When the electric field has two components $E_x$ and $E_z$, the DC offset occurring in the FDTD simulation has to be taken into account [P2,74,75]. A DC current is induced to the perfectly conducting metal, and thus constant components are added to the oscillating field values. The constant terms can be filtered by post-processing.

Updating equations are composed as in three-dimensional case, except, that the *y*-direction, i.e., the index *r*, is dropped out. For example, the updating equation for the electric field component $E_x$ in two-dimensional case is

$$E_x^{n+1}(q,s) = \frac{2\varepsilon - \Delta t\sigma}{2\varepsilon + \Delta t\sigma} E_x^{n}(q,s) - \frac{2\Delta t}{2\varepsilon + \Delta t\sigma}\left[\frac{1}{\Delta z}(H_y^{n+\frac{1}{2}}(q,s+\tfrac{1}{2}) - H_y^{n+\frac{1}{2}}(q,s-\tfrac{1}{2}))\right]. \quad (3\text{–}19)$$

### 3.1.3 Choice of discretisation steps

The error of the central difference approximation is of the order of $O(\Delta^2)$, where $\Delta$ is the discretisation step in time or in space. Thus, the smaller the discretisation steps are the smaller is the error in the computation. In addition, to minimize the discretisation error, there are two other criteria for choice of discretisation steps: 1) the stability of the calculation sets a condition to the time step and 2) the minimization of numerical dispersion sets a condition to the grid spacing. Also, the discretisation steps in space have to be small enough for modelling appropriately the studied structure.

The discretisation used in the Yee's cell leads to an explicit time integration. Therefore the algorithm is not stable with an arbitrary time-step but there is a maximum value for the time-step. The Courant's stability criterion can be written as [76,77]:

$$\Delta t = \frac{1}{C_0 c\sqrt{\frac{1}{\Delta x^2} + \frac{1}{\Delta y^2} + \frac{1}{\Delta z^2}}}. \quad (3\text{–}20)$$

The Courant's number $C_0 \geq 1$ should be kept as small as possible to save the computation time and to minimize the numerical dispersion error [76,77].

The discretisation of the calculation domain produces numerical dispersion. If the maximum allowable numerical dispersion is 1 %, the maximum grid spacing is about $\lambda/18$ [78].

Non-uniform grid is used because the hologram structure contains slots of different widths and because it is very large in wavelengths. Very small grid spacing is used near the slot edges and a coarser grid is used in the centre areas of slots and metal strips. The varying grid spacing has to be taken into account in the updating equations. In two-dimensional case, the partial derivative with respect to the *x*-coordinate is approximated as:

$$\frac{\partial E(q,s)}{\partial x}\Big|_{x=x_0} \approx \frac{E(q+\frac{1}{2},s)-E(q-\frac{1}{2},s)}{\frac{1}{2}(\Delta x(q+\frac{1}{2})+\Delta x(q-\frac{1}{2}))}, \tag{3–21}$$

where the grid spacing depends on the calculation point. The difference between the sizes of the adjacent cells causes additional error to the calculation. A rule of thumb is to keep the ratio between sizes of two adjacent cells in the range 0.5–2.0 [79]. In the hologram simulations, a uniform grid size is used for the *z*-direction.

### 3.1.4 PML absorbing boundary conditions

The excitation brings energy to the calculation domain, while the absorbing boundaries let the energy go out and keeps the system stable. Therefore appropriate absorbing boundary conditions (ABC) are very important in the FDTD simulations. With good absorbing boundaries the edges of the calculation domain can be brought near the studied structure. Thus, the size of the calculation domain is decreased and, further, the computation time is reduced.

The first absorbing boundaries for FDTD were based on differential operators that allow the outgoing wave to propagate through the calculation boundary but inhibit the incoming wave and thus the reflection [80,81]. Updating equations of different orders can be formed at the boundaries from the differential operators [81,82]. The super absorption method applied to the above methods improves considerably the performance of the absorbing boundaries [83].

Another approach is to use absorbing layers at the edges of the calculation domain. Magnetic conductivity, which is included in the first Maxwell equation, can be used in the construction of the perfectly matched layer (PML), i.e. the absorbing media, which have the same wave impedance as the free space. Thus, there are no reflections in the interface between the free space and the PML media. On the other hand, the PML media is lossy and the wave damps out. Perfect electric conductor (PEC) boundaries are used in the edges of the calculation domain, which produces reflections. However, the wave has to travel twice through the absorbing layers before it comes back to the free space region. Berenger applied first this technique to the FDTD simulations [73]. Figure 3.1 shows a schematic of a two-dimensional calculation domain with PML absorbing boundaries.

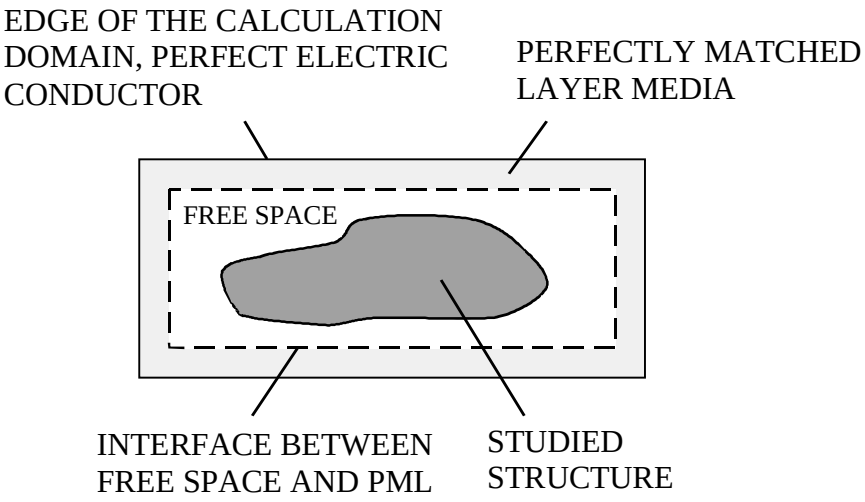


Figure 3.1: Two-dimensional calculation domain with PML absorbing boundaries.

The relation between the non-physical electric and magnetic conductivities for the PML media is

$$\frac{\sigma}{\varepsilon_0} = \frac{\sigma^*}{\mu_0}. \tag{3–22}$$

Large differences in the conductivities between adjacent calculation points produce numerical reflections [73,84]. Therefore near the interface between free space and absorbing media the conductivities have to increase slowly. Usually, the following polynomial distribution for the conductivities is used:

$$\sigma(\rho) = \sigma_m(\rho/\delta)^n, \tag{3–23}$$

where $\sigma_m$ is the maximum value for the conductivity, $\rho$ is the distance from the interface, and $\delta$ is the total thickness of the PML. The larger the exponent of the polynomial is the slower the increase of the conductivity near the interface is. If the exponent is large the conductivity increases rapidly near the outer boundary. However, it is not very critical since the electromagnetic wave is attenuated already in the absorbing media.

The total absorption depends on the integral of the conductivity distribution. If the maximum conductivity is constant, the total absorption depends on the exponent of the polynomial in the following way:

$$\text{Total absorption} \propto e^{-\frac{1}{n+1}}. \tag{3–24}$$

Thus, the total absorption is small when the exponent is large. The choice of the exponent is a trade-off between total absorption and numerical reflections, and it depends on the thickness of the absorbing layer: the thicker is the layer the larger is the exponent [84].

### 3.1.5 Excitation

In the two-dimensional hologram analysis, the system is excited at a line. The excitation field is added to the value from the normal updating equation as follows:

$$E^n(q,s_e) = E^n{}_c(q,s_e) + E^n{}_{exc}(q,s_e), \tag{3–25}$$

where $E^n{}_c(q,s_e)$ is the field value from the updating equation and $E^n{}_{exc}(q,s_e)$ is the excitation field. The waves reflected from the studied structure can pass the excitation line, which can be situated near the studied structure thus reducing the size of the computation domain [85,86].

In the hologram analysis, the excitation is the radiation pattern of the feed horn in the hologram plane. The radiation pattern depends on the frequency and, thus, a sinusoidal excitation at a single frequency is used. A gaussian pulse cannot be used for getting wideband behaviour of the operation. The hologram has to be analysed at several frequencies for finding out the bandwidth of the hologram.

## *3.2 Physical optics*

The result of the FDTD analysis is the aperture field of the hologram. Physical optics (PO) is used to calculate the electric field in the quiet-zone radiated from the hologram aperture. When the simplification for the hologram structure is made and only one line of the hologram is analysed, it is convenient to use two-dimensional physical optics integration formula. When the whole hologram aperture is considered, three-dimensional physical optics formula is used.

### 3.2.1 Two-dimensional case

According to the Huygens' principle the electric field due to radiation of the surface $S'$ is [87]

$$\bar{E}(\bar{r}) = \int_{S'} \left\{ j\omega\mu \bar{\bar{G}}(\bar{r},\bar{r}') \cdot \bar{J}_s(\bar{r}') - \nabla \times \bar{\bar{G}}(\bar{r},\bar{r}') \cdot \bar{M}_s(\bar{r}') \right\} dS', \tag{3–26}$$

where $\overline{\overline{G}}(\bar{r},\bar{r}')$ is the dyadic Green's function, and $\bar{J}_s$ and $\bar{M}_s$ are electric and magnetic surface currents, respectively. The surface $S'$ is reduced to a straight line. In the physical optics approximation, the electric and magnetic fields are transformed to the equivalent electric or magnetic surface currents. Only one of the equivalent surface current components is needed: $\bar{J}_s(\bar{r}') = 2\bar{n} \times \bar{H}_a(\bar{r}')$ or $\bar{M}_s(\bar{r}') = 2\bar{n} \times \bar{E}_a(\bar{r}')$ [87,88], where $\bar{n}$ is the normal vector of the aperture.

The formulas can be written separately for vertical and horizontal polarisations. When the electric field of the aperture is vertically or *y*-polarised, the electric field in the quiet-zone extent is expressed as

$$\bar{E}(\bar{r}) = -2jk\int_{S'}\sqrt{\frac{2}{\pi k|\bar{r}-\bar{r}'|}}e^{j(k|\bar{r}-\bar{r}'|-\frac{\pi}{4})}E_a(\bar{r}')\bar{u}_y\,dS'. \tag{3–27}$$

When the electric field of the aperture is horizontally or *x*-polarised, the electric field in the quiet-zone extent is

$$\begin{aligned}\bar{E}(\bar{r}) = -2jk\int_{S'}E_a(\bar{r}')\sqrt{\frac{2}{\pi k\rho}}e^{j(k\rho-\frac{\pi}{4})}\cdot \\ \left\{\left(1-\frac{(x-x')^2}{\rho^2}-\frac{j}{k\rho}\right)\bar{u}_x+\frac{(x-x')(z-z')}{\rho^2}\bar{u}_z\right\}dS',\end{aligned} \tag{3–28}$$

where $\rho = |\bar{r}-\bar{r}'|$.

### 3.2.2 Three-dimensional case

In the three-dimensional case, the radiating field from the aperture is written as [87]

$$\bar{E}(\bar{r}) = -\int_{S'}\nabla g(\bar{r},\bar{r}')\times\bar{M}_s(\bar{r}')dS', \tag{3–29}$$

where $g(\bar{r},\bar{r}')$ is the scalar Green's function. It is convenient to write separate formulas for two different aperture field polarisations also in three-dimensional case. The radiated field in the quiet-zone extent for the *y*-polarised aperture field is

$$\bar{E}(\bar{r}) = \int_{S'}E_a(\bar{r}')\frac{1+jkR}{2\pi R^3}e^{-jkR}\{(z-z')\bar{u}_y-(y-y')\bar{u}_z\}dS'. \tag{3–30}$$

For the *x*-polarised aperture field the radiated field is

$$\bar{E}(\bar{r}) = \int_{S'} E_a(\bar{r}') \frac{1+jkR}{2\pi R^3} e^{-jkR} \{(z-z')\bar{u}_x - (x-x')\bar{u}_z\} dS'. \quad (3\text{–}31)$$

## 3.3 Simplified models for the hologram

The hologram includes very fine details compared to the wavelength and, simultaneously, its largest dimensions are always at least several hundreds of wavelengths. The discretisation of the whole hologram structure for numerical calculations is not feasible. Two approaches for simplifying the hologram structure are used:

1) Only one horizontal cut of the hologram is simulated at a time, and the quiet-zone field radiated by the hologram is calculated at the same horizontal plane where the hologram cut has been taken. The operation of the whole hologram is achieved by simulating several horizontal cuts of the hologram. The simulation method based on this simplification is presented in [P2].

2) Transmissions of the electromagnetic wave through slots of a periodic structure are studied. The hologram structure is binarized with a finite step size and, thus, the slot widths are quantized to have discrete values. Transmissions for all slot widths and for two linear polarisations are calculated. Finally, the transmissions are applied to the calculation of the whole hologram structure. The simulation method based on this simplification is presented in [P5].

The first one is more accurate and it is used when the holograms are designed [P1,P2]. The transmission of the electromagnetic wave through the hologram slots depends on the polarisation, and the curvature of the slots causes cross-polarisation. The first simplification method is not applicable for predicting cross-polarisation, because it is not capable for taking into account the curvature of the slots. Instead, the second method provides a tool for cross-polarisation calculations [P5]. The transmission of the electromagnetic wave through a narrow slot is studied with two-dimensional FDTD. The method of moments can also be used for this type of analysis [1,89,90].

# 4 Design of the hologram for a CATR

## 4.1 Hologram binarization

The hologram is generated numerically with a computer (CGH, computer generated hologram) when the incident field and the desired field are known. In an ideal case, the transmission of the hologram can be changed continuously, but in practice there are no suitable materials or manufacturing techniques for accomplishing this. Therefore the hologram pattern has to be binarized. The binarized hologram pattern can be generated numerically from the following formula [60,61]:

$$T_B(x',y') = \begin{cases} 0, & \text{when } 0 \le \frac{1}{2}\left[1+\cos\Psi(x',y')\right] \le b, \\ 1, & \text{when } b < \frac{1}{2}\left[1+\cos\Psi(x',y')\right] \le 1, \end{cases} \tag{4–1}$$

where $\Psi(x',y') = \varphi(x',y') + 2\pi\nu$ is the phase term. The term $\varphi(x',y')$ is the normalised phase of the incident field in the hologram plane. The spatial carrier frequency $\nu$ determines the propagation direction of the plane wave according to $\theta = \arcsin(\nu\lambda)$. The direction of 33° is chosen in order to avoid the disturbance of the diffraction modes, which propagate to the direction of the hologram normal.

The parameter $b$ is calculated as

$$b = 1 - (1/\pi)\arcsin a(x',y'), \tag{4–2}$$

where the function $a(x',y')$ depends on the relation between the amplitudes of the desired wave front and the incident field in the aperture. It compensates the amplitude of the incoming field so that the amplitude of the aperture field is appropriate. In practice the function $a(x',y')$ is written as

$$a(x',y') = \frac{W(x',y')}{\left|\overline{E}_{\text{feed}}(x',y')\right|}, \tag{4–3}$$

where $\overline{E}_{\text{feed}}(x',y')$ is the field of the incident wave front in the hologram plane and $W(x',y')$ is the weighting function.

## 4.2 Optimisation of the hologram

The electromagnetic wave has interactions in the slots so that the transmission of the incoming field is not binarized. Usually, the hologram, which is generated assuming

the ideally binarized transmission, does not radiate an appropriate wave front for antenna measurements. However, the generation of the hologram can be changed in such a way that the hologram produces a plane wave that meets its requirements in the quiet-zone. Typical requirements for the quiet-zone field are maximum deviations of ±0.5 dB and ±5° in amplitude and phase, respectively.

The optimisation of the hologram is an iterative procedure that can be divided into the following four parts [P1,91]:

1) The weighting function is chosen. The weighting function controls the widths of the slots and thus basically determines the amplitude pattern of the quiet-zone field.

2) The hologram pattern is generated with a computer.

3) The quiet-zone field radiated by the hologram is simulated with a combined FDTD and PO method. If the amplitude of the plane wave does not meet the requirements, we have to go back to step 1 and choose a new weighting function.

4) The phase of the quiet-zone field can be adjusted by changing the angle of the plane wave in different parts of the hologram (i.e., by changing the spatial carrier frequency). This affects the locations of the slots. After a phase correction we go back to step 2 and generate a modified hologram.

### 4.2.1 Weighting function

The weighting function for the plane wave in an ideal case would be $W(x', y') = 1$. However, this would not produce a properly operating hologram. One major task of the weighting function is the tapering of the hologram aperture field for preventing the disturbance of the edge diffraction in the quiet-zone. As a consequence, the widths of the slots are narrower near the edges of the hologram. Due to the binarization of the hologram, the tapering is not continuous in the horizontal or *x*-direction as it is in the vertical direction. However, the used width of the total tapering area is essentially the same all over the hologram.

Usually, the weighting function with the edge tapering is still not sufficient for an adequate hologram operation, but local changes have to be done. The increase of the weighting function widens the slots in the corresponding part of the hologram. In practice, it is proven that the slot widths should be smaller than one half of the wavelength. With larger slot widths the transmission through the slots does not increase as linearly as with smaller slot widths and the optimisation becomes very difficult. Different weighting functions are described in [P1,5,10].

The shape of ellipse is advantageous for the holograms, as part of the hologram size is lost in the *x*-direction due to the propagation direction different from the hologram normal. With the propagation angle of 33° the projection of the hologram is about 16 % smaller than the hologram.

### 4.2.2 Transfer of the feed

For a hologram CATR, which is already in operation, the transfer of the feed has importance in two cases. Firstly, the main beam of a high-gain AUT can be measured by scanning the feed transversally. Secondly, when the operating frequency of the CATR is changed, the phase pattern of the quiet-zone field can be compensated with an axial feed movement. An example of the phase compensation is presented in [P3].

However, the feed transfer has relevance also in the hologram optimisation. The following two ways are applied for facilitating the designing of the hologram and, furthermore, for improving the performance of the hologram:

1) Feed rotation in the *xz*-plane (Figure 4.1 a)). The phase centre of the feed horn is not moved, thus the phase of the quiet-zone field is not affected. However, the illumination of the hologram is not symmetric. As a consequence, an amplitude tilt of even a few decibels in the quiet-zone field can be corrected.

2) Feed offset in the *x*-direction (Figure 4.1 b)). Although the feed horn is directed to the hologram normal direction, it has a transversal offset so that it does not point to the hologram centrepoint. For example, an offset of 0.1 m has been used for a 0.6 m hologram [14]. The transversal feed transfer can also be seen as a transfer of the generation area of the hologram. In principle, the hologram could be generated in any place when the incident wave front and the desired wave front are known. The transversal feed transfer is a usable tool if the amplitude of the quiet-zone field does not behave properly on the other side of the quiet-zone. Usually, the quiet-zone side corresponding to the wider slot widths behaves worse and it is advantageous to move the generation area a little to the other direction. A major drawback is the increased spill-over in the other side of the hologram.

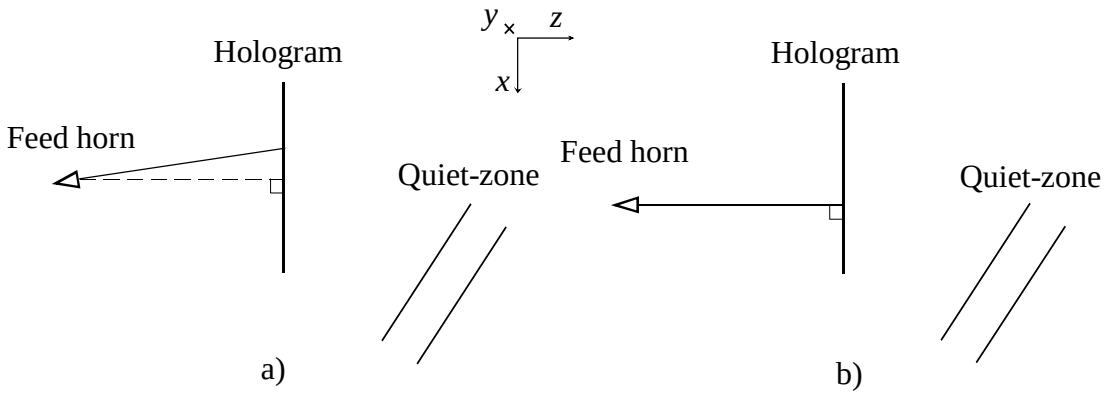


Figure 4.1: a) Rotation of the feed horn and b) offset of the feed horn.

### 4.2.3 Optimisation of the phase

The optimised weighting function makes the amplitude pattern of the quiet-zone field flat. The same goal is with the feed rotation and the feed offset. These actions affect also the phase of the quiet-zone field and therefore phase may have to be corrected. The feed transfer in the *z*-direction gives means for the frequency compensation. However, the main tool in the phase optimisation is the change of the angle of the plane wave direction $\theta$ (or the spatial carrier frequency $v$) in different parts of the hologram. The change of the plane wave direction affects the places of the hologram slots. The changes are of the order of 0.001° [5].

The correction of the phase affects also the amplitude and therefore the quality of the amplitude pattern has to be checked. In this stage, the needed modifications to the weighting function are usually quite small [10].

### 4.2.4 Optimisation in the *y*-direction

The FDTD-simulation used in the hologram optimisation gives the aperture field only at one line parallel with the horizontal or *x*-axis. The best result is obtained when the line under study is the centreline of the hologram, i.e. $y = 0$. The farther away the line from the centreline is the larger the error made in the quiet-zone field prediction is, because the slot curvatures increase.

In the optimisation of the hologram pattern, the starting point is in the optimisation of the centreline. After the best possible operation in the middle of the hologram is found, the hologram is optimised at other lines. Cuts of the hologram with appropriate distances are taken, and the slots of the cut are assumed as vertical without curvature. The quiet-zone field is calculated at the same *xz*-plane where the cut has been taken ($y = y_1$, see Figure 2.5).

In practice, there is no need for very large changes in the weighting function to achieve an adequate operation of the hologram in the vertical direction. Usually, it is sufficient to confirm that the quiet-zone field quality is appropriate at few different *y*-levels.

# 5 Summary of publications

Paper [P1] describes the compact antenna test range based on a hologram. The advantage of the use of a hologram instead of a reflector in a CATR is the less stringent surface accuracy requirement. In addition, a hologram is relatively easy to fabricate and therefore manufacturing costs are reduced compared to those of reflectors. In the paper, the synthesis and features of the computer-generated holograms are briefly reviewed. The operation of the hologram in antenna measurements is described and it is demonstrated by experiments at 119 GHz. For a 550 mm demonstration hologram, the theoretical peak-to-peak amplitude and phase deviations are 0.4 dB and 5°, respectively, and experimental peak-to-peak deviations are 0.8 dB and 10°. The work described in [P1] is an extension to the work made by Tuovinen, Vasara, and Räisänen [33]. Taavi Hirvonen was responsible for the preparation of the paper, and he made all the measurements. This author was responsible for the theoretical analysis of the hologram. The design of the demonstration hologram was a result of co-operation of Taavi Hirvonen and this author. Jussi Tuovinen was a co-supervisor.

Paper [P2] deals with the numerical analysis of the hologram CATR and it is closely related to [P1]. The previously used method uses binary transmission when evaluating transmission of the electromagnetic wave through the hologram structure [33]. A new method for calculating the transmission through a horizontal cut of a hologram is described. The FDTD method is applied to a non-uniform, i.e., non-periodical grating. The aperture field of the hologram is obtained as the result of the FDTD simulation. The physical optics method is used for calculating the radiation of the aperture. The theoretical analysis method is validated with experiments at 119 GHz. The operation of holograms designed on the basis of the previous and the new analysis method are compared showing the necessity of an adequate analysis method. This author was responsible for the preparation of this paper and made all the theoretical simulations. Taavi Hirvonen was responsible for all the measurements, he designed the hologram based on the binary transmission, and he wrote the physical optics code. Jussi Tuovinen was a co-supervisor.

Paper [P3] consists of a theoretical tolerance analysis made at 500 GHz for studying the feasibility of the hologram CATR for submillimetre wavelengths. The tolerance analysis is based on the analysis method described in [P2] and the optimisation of the hologram used in the analysis is reported in [8]. The main emphasis is on the effects of systematic and random errors occurring in hologram manufacturing process. The feed displacement, frequency and polarisation changes, and the joints between the parts of the hologram are also discussed. The accuracy requirements for the hologram

pattern depend on the required field quality in the quiet-zone extent. The standard wet etching technique is seen as a feasible method for up to 500 GHz. The problem is the required large size of the hologram in practical antenna measurements. If the hologram is made of several pieces, the pieces have to be aligned accurately. Otherwise, the pieces are 'out of phase' so that they radiate the plane waves in slightly different directions. A more detailed study on the effects of the gaps between hologram pieces and the tape used in the splicing the pieces is presented in [14]. An adequate planarity of the hologram is achieved by stretching the hologram in a frame. The hologram material has to be handled with care for preventing mechanical damages, e.g., wrinkles, which remain despite the stretching. The phase curvature due to a frequency change can be compensated with an axial feed movement. However, the bandwidth of the hologram is limited to less than ±10 %. The hologram is very polarisation sensitive and it has to be optimised for one linear polarisation. Taavi Hirvonen was mainly responsible for the preparation of the paper. This author carried out all the theoretical calculations.

Paper [P4] deals with the effects of the planarity errors of the hologram and it is an continuation of paper [P3]. A simple theoretical approximation for the phase error in the quiet-zone field is derived. The approximation is based on changed path lengths due to planarity errors. According to the path length approximation, the planarity error of the hologram can be about 12 times that of the surface error of a reflector. In addition, theoretical simulations are also carried out. Locally, the simulated peak phase errors are smaller than the simple path length approximation predicts. However, the simulations show that planarity error affects the field everywhere in the quiet-zone extent. The errors in the quiet-zone field are proportional to the width (area) and depth of the planarity error. This author was responsible for preparation of the paper and carried out all the simulations. Taavi Hirvonen was a co-supervisor.

Paper [P5] presents another numerical method for the hologram analysis. The whole hologram structure with curved slots can be taken into account. Thus, it is capable of predicting the cross-polarisation performance of the hologram. The theoretical method is validated by comparison with measurements at 39 GHz and 310 GHz. A good agreement between the theoretical and experimental results is seen. The maximum measured cross-polarisation level is about −20 dB at the quiet-zone volume. This author was responsible for the preparation of the paper and carried out all the simulations. The measurements at 39 GHz were made in co-operation with this author and Tomas Sehm. Jussi Säily carried out the measurements at 310 GHz.

Paper [P6] describes the design and manufacturing of the hologram that is used to measure a low-profile link antenna [34,92] at 39 GHz. In this paper, a two-dimensional formula for physical optics calculation is presented, and a choice of the two- or three-dimensional formula in the hologram simulations is discussed. The

results of the first actual antenna measurement carried out with the hologram CATR are also presented. A 22 cm × 2 cm linear antenna array, which is a development version for the link antenna, is measured at 39 GHz. For comparison, the array is measured with the planar near-field scanning method. The results from the hologram CATR and near-field scanning measurements agree very well. This author was responsible for the preparation of the paper. This author designed the holograms and wrote the modified code for the two-dimensional PO analysis. Taavi Hirvonen carried out the hologram CATR and planar near-field measurements.

Paper [P7] presents the results of the measurements of the low-profile antenna array consisting of 256 radiating elements [34]. The design of the hologram made for the measurements is described in [P6]. A comparison between the far-field, the near-field, and the hologram CATR measurement methods is made. The pattern measurements agree well. The gain values obtained from the far-field and near-field measurements agree also very well, but the gain measured with the hologram CATR is about 2 dB lower. This is seen to be due to the large amplitude and phase ripples in the quiet-zone. The measured amplitude ripple is 2.1 dB as the theoretical ripple is only 0.5 dB. The additional error is due to the hologram manufacturing and the reflections in the measurement site. The hologram is made of three pieces, thus, the joining made with tape and incomplete alignment cause additional errors. Also, there are manufacturing errors in the hologram pieces. In spite of the huge amount of the absorbers for preventing stray radiation, the reflections from the concrete walls of an ordinary laboratory facility produce disturbance to the quiet-zone. Tomas Sehm was mainly responsible for the preparation of the paper and he made the far-field and the near-field measurements. Tomas Sehm and this author carried out the hologram CATR measurements together. This author designed the hologram for the measurements. Taavi Hirvonen was a co-supervisor.

Paper [P8] presents the development work of the hologram CATR for the measurements of the Odin telescope and the results of the actual measurements at 119 GHz in Linköping, Sweden, in August 1998. The diameter of the main reflector is 1.1 m and the hologram designed and fabricated for the measurements is 2.4 m × 2.0 m. The hologram is made of seven pieces spliced together with polyester tape. The maximum deviation of the measured amplitude pattern in the quiet-zone is about 3 dB, but in most parts the deviation is within 1.5 dB. The theoretical peak-to-peak amplitude and phase ripples are less than 1 dB and 10°, respectively. However, the measured quiet-zone field is considered to be adequate for the Odin tests. The design and manufacturing of the hologram are described more thoroughly in [10]. The measured and theoretical radiation patterns of the Odin telescope are in good agreement in the main beam region. The effects of the imperfections in the quiet-zone field and in the aperture field of the AUT on the measurements are simulated. As a result, the asymmetric aperture field of the Odin telescope and the imperfect quiet-

zone field increase the level of the first sidelobe. This author was mainly responsible for the preparation of the paper. Taavi Hirvonen and Petri Piironen were responsible for the antenna measurements, albeit this author participated also the measurement group. Taavi Hirvonen and this author designed the hologram for the measurements together. This author made all the antenna measurement simulations. Arto Lehto, Jussi Tuovinen, Antti Räisänen, and Urban Frisk gave useful advice and comments on the interpretation of the measurement results.

Paper [P9] presents the results of the quiet-zone field verification for the submillimetre wave hologram CATR at 310 GHz. The hologram CATR operation, including instrumentation, is demonstrated at submillimetre wavelengths. The capability of the conventional wet-etching technique for hologram manufacturing for high frequencies is studied. The manufacturing succeeded reasonably well and the measured peak-to-peak ripples are 1.0 dB and 10° in the amplitude and the phase, respectively, while theoretical ripples are 0.8 dB and 5°. The design of the 600 mm hologram and the manufacturing are described more thoroughly in [14] and [15]. Jussi Säily was responsible for the preparation of the paper and for all the measurements. This author designed the hologram and made all the theoretical simulations. Janne Häkli assisted in the measurements. Jussi Tuovinen and Arto Lehto were co-supervisors.

# 6 Conclusions

Reflectors are widely used as collimating elements in CATRs, but the surface accuracy requirements become very stringent at millimetre and submillimetre wavelengths. A binary amplitude hologram is a potential alternative for the reflector as the planarity requirements are not as stringent. Furthermore, it is easier to manufacture holograms than reflectors, thus the manufacturing costs are reduced. A drawback is that the performance of the hologram depends strongly on the polarisation and the hologram has to be designed for the operation at one linear polarisation. Another disadvantage is the limited bandwidth: about ±5–10 % depending on the requirements of the quiet-zone field quality.

In this thesis, numerical techniques for analysing the radio frequency hologram are developed. The first analysis technique is adequate for designing holograms for the compact antenna test range application and for studying the performance of the hologram CATR. The second technique is capable of predicting the cross-polarisation levels of the hologram CATR.

The analysis techniques are based on the finite difference time domain and the physical optics methods. The FDTD method is used to calculate the transmission of the electromagnetic wave through the hologram. The physical optics method is then used for calculating the radiation of the resulting aperture field to the quiet-zone extent.

Holograms are always very large in wavelengths therefore simplifying models are made for enabling numerical calculations. In the first model, only one cut of the hologram is simulated at a time. This approach leads to the assumption that the slots of the hologram are straight, parallel, and of infinite length. Experimental results show that this method of analysis is capable of designing holograms for CATR application. Typical design goals for the amplitude and phase of the quiet-zone field are peak-to-peak ripples less than 1.0 dB and 10°, respectively, and they are also achievable in practice. In the second model, the hologram structure is not changed but the slot transmissions are calculated first for a simplified structure and then applied to the whole hologram structure. When the curvatures of the hologram slots and the transmissions for two perpendicular linear polarisations are taken into account, the cross-polarisation produced by the hologram can be calculated. According to the theoretical analysis and the experiments made at 39 and 310 GHz, the maximum cross-polarisation level is about –20 dB in the quiet-zone volume.

Antenna measurements were carried out at 39 and 119 GHz using hologram type CATRs. The measurement results at 39 GHz were compared with those from the planar near-field measurements and the far-field measurements. Good agreement between the radiation patterns was observed. At 119 GHz, the measured radiation pattern of the 1.1 m Odin-telescope agreed well with the theoretical one in the main beam region. The measurements also verified the symmetry of the main beam. The practical antenna measurements proved the applicability of the hologram type of CATR for millimetre wave antenna measurements.

Developed analysis method was used for the theoretical study of the feasibility of the hologram CATR for submillimetre wavelengths. According to the simulations, the accuracy of conventional wet etching technique used for circuit boards is found to be adequate for manufacturing holograms for frequencies up to about 500 GHz. A problem in the wet etching that uses a mask for the exposure of the photo resist is that the narrowest slots are not etched properly. Slots narrower than about 100 μm cannot be etched open at all. This is a problem when realising a taper for submillimetre wavelengths. However, a laser exposure of the photo resist is seen as a method capable of etching narrower slots. The accuracy of the laser exposure process is expected to be sufficient up to 1 THz.

A major problem in the manufacturing is the large sizes, which are required for the holograms used in practical antenna measurements. Preferably, the hologram should be made of one piece but this may not be possible in the case of large holograms. The alignment of the several pieces of the hologram has to be made accurately. Also, the glues and tapes used in the joining have to be electrically as invisible as possible. The manufacturing of large holograms is seen the most critical issue in the development of the hologram CATR. These fabrication issues must be resolved before this approach becomes practicable for demanding antenna measurements.

The key issues in future hologram development besides hologram manufacturing are: 1) study of the use of a dual reflector feed system for shaping the illumination of the hologram, 2) further development of the numerical methods for taking into account the whole hologram structure, and 3) simulation of the antenna measurements for studying the performance of the hologram CATR in the cross-polarisation measurements. By shaping the illumination of the hologram, the amplitude taper would be accomplished with the feed rather than with the hologram. Thus, the hologram would not contain very narrow slots and the manufacturing process would be easier. In addition, the sensitivity to the polarisation may be reduced [4]. Further development of hologram analysis may also be based on numerical methods other than the FDTD, like the finite element method (FEM) or the method of moments (MOM).

# Errata

In [P1] on page 5 the caption of Figure 8 should read “Fig. 8. A Two-dimensional (2-D) measurement result …”.

In [P2] on page 3 in equation (11) the term $E_e^n(i,k_e)$ should read $E_c^n(i,k_e)$.

In [P2] on page 3 in equation (12) the term in the brackets should read $[(z-z')\overline{u}_y-(y-y')\overline{u}_z]$.

In [P2] on page 3 in Figure 6 the “measured” phase is marked with bullets and the “FDTD” phase is marked with a solid line.

In [P4] on page 4 the caption of Figure 2 should read “**Figure 2.** The quiet-zone fields, effect of **a)** the depth (nominal(–), $h_d$ =0,08$\lambda$(□), 0,16$\lambda$ (*), 0,24$\lambda$ (o)) and **b)** the width (nominal (–), $w_d$ = 4 cm(□), 6 cm (*), 8 cm (o)) of the planarity error.”

In [P9] on page 2 the title of the Fig. 4 should read “quiet-zone of 310 GHz CATR”.

# References


[1] J. Tuovinen, T. Hirvonen, J. Ala-Laurinaho, A. Lehto, A. Räisänen: Test method of the Odin satellite 1.1 m antenna at 119 and 500 GHz: Progress report, *ESTEC/EMSL Workshop on Large Microwave Measurement Facilities*, Noordwijk, The Netherlands, 1995, pp. 41–53.

[2] J. Ala-Laurinaho, T. Hirvonen, J. Tuovinen, A. V. Räisänen: The simulation of a hologram CATR with FDTD, *Proceedings of the URSI/IEEE/IRC XXI National Convention on Radio Science*, Espoo, Finland, 1996, pp. 85–86.

[3] T. Hirvonen, J. Ala-Laurinaho, J. Tuovinen, A. V. Räisänen: Development of a hologram CATR, *Proceedings of the URSI/IEEE/IRC XXI National Convention on Radio Science*, Espoo, Finland, 1996, pp. 61–62.

[4] P. R. Foster, D. Martin, C. Parini, A. Räisänen, J. Ala-Laurinaho, T. Hirvonen, A. Lehto, T. Sehm, J. Tuovinen, F. Jensen, K. Pontoppidan: Mmwave antenna testing techniques - Phase 2, *MAAS Report 304*, Issue No 2, ESTEC Contract No 11641/95/NL/PB(SC), December 1996, 224 p.

[5] T. Hirvonen, P. Piironen, J. Ala-Laurinaho, A. Lehto, A. V. Räisänen: Hologram CATR for mm- and submm-wavelengths: A progress report, *Proceedings of the 8th International Symposium on Space Terahertz Technology*, Cambridge, MA, 1997, pp. 490–498.

[6] J. Ala-Laurinaho, P. R. Foster, G. J. Junkin, T. Hirvonen, A. Lehto, D. H. Martin, A. D. Olver, R. Padman, C. Parini, A. V. Räisänen, T. Sehm, J. Tuovinen, R. J. Wylde: Comparison of antenna measurement techniques for 200 to 1500 GHz (invited paper), *Proceedings of the 20th ESTEC Antenna Workshop on Millimetre Wave Antenna Technology and Antenna Measurements*, Noordwijk, The Netherlands, 1997, pp. 345–351.

[7] T. Hirvonen, J. Ala-Laurinaho, A. Lehto, J. Tuovinen, A. V. Räisänen: Feasibility of a hologram CATR for measuring large mm- and submm-wave antennas, *Proceedings of the 20th ESTEC Antenna Workshop on Millimetre Wave Antenna Technology and Antenna Measurements*, Noordwijk, The Netherlands, 1997, pp. 355–362.

[8] J. Ala-Laurinaho, T. Hirvonen, A. V. Räisänen: Optimization of a submillimeter wave hologram CATR, *Proceedings of the 1997 AP-S International Symposium*, Montréal, Canada, 1997, pp. 136–139.

[9] T. Sehm, T. Hirvonen, J. Ala-Laurinaho, A. V. Räisänen: Measurement of a novel 40 GHz planar antenna using planar near-field scanning techniques and a hologram CATR, *Proceedings of the 27th European Microwave Conference*, Jerusalem, Israel, 1997, pp. 880–885.

[10] T. Hirvonen, J. Ala-Laurinaho, P. Piironen, J. Tuovinen, J., A. V. Räisänen: A 119 GHz CATR based on a 2.4 m hologram, *Proceedings of the 19th Meeting and Symposium of AMTA*, Boston, MA, 1997, pp. 164–169.

[11] A. V. Räisänen, T. Hirvonen, T. Sehm, J. Ala-Laurinaho, A. Lehto: Feasibility of different antenna measurement techniques at submillimeter wavelengths (invited paper), *Proceedings of the International Conference on Microwave and Millimeter Wave Technology ICMMT'98*, Beijing, China, 1998, pp. 367–371.

[12] A. V. Räisänen, T. Hirvonen, J. Ala-Laurinaho, A. Lehto: Hologram as the collimating element in a compact antenna test range at millimeter wavelengths (invited paper), *Proceedings of the SPIE's International Symposium on Optical Science, Engineering, and Instrumentation*, San Diego, CA, 1998, Vol. 3464, pp. 212–221.

[13] A. V. Räisänen, T. Hirvonen, T. Sehm, J. Ala-Laurinaho, A. Lehto: Measurements of high gain antennas at millimeter wavelengths using a hologram CATR (invited paper), *Proceedings of the Third International Kharkov Symposium "Physics and Engineering of Millimeter and Submillimeter Waves"*, Kharkov, Ukraine, 1998, pp. 35–39.

[14] J. Ala-Laurinaho, J. Säily, J. Häkli, J. Tuovinen, A. Lehto, A. V. Räisänen: Design of a 310 GHz hologram compact antenna test range, *Proceedings of the 22nd ESTEC Antenna Workshop on Antenna Measurements*, ESTEC, Noordwijk, The Netherlands, 1999, pp. 159–162.

[15] J. Säily, J. Ala-Laurinaho, J. Häkli, J. Tuovinen, A. Lehto, A. V. Räisänen: Development of a 310 GHz Hologram Compact Antenna Test Range, *Proceedings of AMTA'99, Meeting and Symposium of Antenna Measurements Association*, Monterey Bay, CA, 1999, pp. 464–469.

[16] J. Häkli, J. Ala-Laurinaho, J. Säily, J. Tuovinen, A. Lehto, A. V. Räisänen: Hologram compact antenna test range for submillimetrewave region, *Proceedings of the URSI/IEEE/IRC XXIV National Convention on Radio Science*, Turku, Finland, 1999, pp. 34–35.

[17] A. V. Räisänen, J. Ala-Laurinaho, J. Säily, J. Häkli: Millimeter and submillimeter wave antenna testing with a hologram CATR (invited paper), accepted for publication in *Proceedings of the COST-712 Workshop on Techniques and Facilities in the mm and submm Range for Atmospheric Research*, Bern, Switzerland, 1999.

[18] J. Säily, J. Ala-Laurinaho, J. Häkli, J. Tuovinen, A. Lehto, A. V. Räisänen: Facility for compact antenna test ranges for submillimeter wavelengths, *Proceedings of the 11th International Symposium on Space Terahertz Technology*, Ann Arbor, MI, USA, 2000, pp. 590–597.

[19] J. Tuovinen, J. Ala-Laurinaho, J. Säily, J. Häkli, A. Lehto, A. V. Räisänen: Hologram - modern optics for millimetre and submillimetre wave antenna

testing, *Proceedings of the AP2000 Millennium Conference on Antennas and Propagation*, Davos, Switzerland, 2000, paper No. 0070.

[20] A. V. Räisänen, T. Sehm, A. Lehto, J. Ala-Laurinaho: Low-profile solutions for high-gain antennas and their measurements at millimeter wavelengths, *Proceedings of the XII International Conference on Microwaves, Radar, and Wireless Communications MIKON-2000*, Wroclaw, Poland, 2000, pp. 183–188.

[21] J. Ala-Laurinaho, J. Häkli, A. Lehto, P. Piironen, A. Räisänen, J. Säily, J. Tuovinen: *Submillimetre wave antenna testing using a hologram CATR: Abstract, Summary Report, and Task Reports*, ESTEC Contract No. 13096/98NL/SB, June 2000, 92 p.

[22] F. von Schéele: The Swedish Odin satellite to eye heaven and earth, *47th International Astronautical Congress IAF*, 1996.

[23] *FIRST, Far Infra-Red and Submillimetre Space Telescope*, ESA Document, SCI(93)6, September 1993, 123 p.

[24] *COBRAS/SAMBA, A Mission Dedicated to Imaging the Anisotropies of the Cosmic Microwave Background, Report on the Phase A Study*, ESA Document, D/SCI(96)3, February 1996, 115 p.

[25] A. Ouisse, P. De Maagt, D. Lamarre, G. Padovan: MASTER antenna requirements: some investigations, *Proceedings of the 20th ESTEC Antenna Workshop on Millimetre Wave Antenna Technology and Antenna Measurements*, Noordwijk, The Netherlands, 1997, pp. 75–85.

[26] *Sub-mm Observation of Processes in the Atmosphere (SOPRANO)*, Daimler-Benz Aerospace Report, No. FR SOP-0000-01 DOR of 20/04/95. Issued under ESTEC Contract No. 10621/93/NL/SF.

[27] J. Tuovinen: Methods for testing reflector antennas at THz Frequencies, *IEEE Antennas and Propagation Magazine*, Vol. 35, No. 6, 1993, pp. 7–13.

[28] P. R. Foster (ed.): Mmwave antenna testing techniques, *MAAS Report 281*, Issue No 1, ESTEC Contract No 11641/95/NL/PB(SC), January 1996.

[29] J. Aurinsalo, S. Karhu, A. Koivumäki, R. Pitkäaho, A. Lehto, A. Räisänen, T. Tolmunen, J. Tuovinen: *Test methods and ranges for testing the millimeter wave sounder of the Meteosat second generation satellites, Final Report*, ESTEC Contract No. 7966/88/NL/PB(SC), 1990.

[30] T. Sehm, A. Lehto, J. Tuovinen, A. V. Räisänen: Planar near-field scanning measurements of large antennas at terahertz frequencies, *Proceedings of the 20th ESTEC Antenna Workshop on Millimetre Wave Antenna Technology and Antenna Measurements*, Noordwijk, The Netherlands, 1997, pp. 305–312.

[31] C. G. Parini, A. D. Olver: The use of reflector CATR for antenna measurements in the region of one terahertz, *Proceedings of the 20th ESTEC Antenna*

*Workshop on Millimetre Wave Antenna Technology and Antenna Measurements,* Noordwijk, The Netherlands, 1997, pp. 371–378.

[32] J. Habersack, J. Hartmann, J. Lemanczyk, P. De Maagt, H.-J.Steiner: Facility trade-off for measurements up to 500 GHz, *Proceedings of the Twenty-Second Meeting and Symposium of Antenna Measurement Techniques Association (AMTA)*, Philadelphia, PA, 2000, pp. 261–266.

[33] J. Tuovinen, A. Vasara, A. Räisänen: A new type of compact antenna test range, *Proceedings of the 22nd European Microwave Conference*, Espoo, Finland, Vol. 1, 1992, pp. 503–508.

[34] T. Sehm, A. Lehto, A. V. Räisänen: A large planar 39-GHz antenna consisting of an array of waveguide-fed horns, *IEEE Transactions on Antennas and Propagation*, Vol. 46, No. 8, 1998, pp. 1189–1193.

[35] *IEEE Standard Test Procedure for Antennas*, IEEE Std 149-1979, published by IEEE, Inc., 1979, 143 p., distributed by Wiley-Interscience.

[36] V. J. Vokurka: Advanced antenna measurements, *Proceedings of the 14th European Microwave Conference*, Liege, Belgium, 1984, pp. 60–70.

[37] G. R. Birtcher, C. A. Balanis, V. J. Vokurka: RCS measurements, transformations, and comparisons under cylindrical and plane wave illumination, *IEEE Transactions on Antennas and Propagation*, Vol. 42, No. 3, 1994, pp. 329–334.

[38] K. S. Farhat, J. C. Bennett, A. J. T. Whitaker, N. Williams: The semi compact range and its evolution as a fast near-field technique for millimeter-wave applications, *Proceedings of the 14$^{th}$ Meeting and Symposium of the Antenna Measurement Techniques Association (AMTA)*, Columbus, OH, 1992, pp. 5-7–5-12.

[39] K. M. Keen: Satellite antenna measurement techniques, *IEE Proceedings*, Vol. 127, Pt. A, No. 7, 1980, pp. 417–434.

[40] R. C. Hansen: Measurement distance effects on low sidelobe patterns, *IEEE Transactions on Antennas and Propagation*, Vol. 32, No. 6, 1984, pp. 591–594.

[41] G. E. Evans: *Antenna Measurement Techniques*, Artech House, Boston, 1990, 229 p.

[42] A. D. Yaghjian: An overview of near-field antenna measurements, *IEEE Transactions on Antennas and Propagation*, Vol. 34, No. 1, 1986, pp. 30–45.

[43] Y. Rahmat-Samii, L. I. Williams, R. G. Yaccarino: The UCLA bi-polar planar-near-field antenna-measurement an diagnostics range, *IEEE Antennas and Propagation Magazine*, Vol. 37, No. 6, 1995, pp. 16–34.

[44] D. Slater: *Near-Field Antenna Measurements*, Artech House, Boston, 1991, 310 p.

[45] W. H. Kummer, E. S. Gillespie: Antenna measurements – 1978, *Proceedings of the IEEE*, Vol. 66, No. 4, 1978, pp. 483–507.

[46] A. C. Newell: Error analysis techniques for planar near-field measurements, *IEEE Transactions on Antennas and Propagation*, Vol. 36, No. 6, 1988, pp. 769–773.

[47] N. Erickson, V. Tolls: Near-field measurements of the submillimeter wave astronomy satellite antenna, *Proceedings of the 20th ESTEC Antenna Workshop on Millimetre Wave Antenna Technology and Antenna Measurements*, Noordwijk, The Netherlands, 1997, pp. 313–319.

[48] J. Tuovinen, A. Lehto, A. Räisänen: A new method for correcting phase errors caused by flexing of cables in antenna measurements, *IEEE Transactions on Antennas and Propagation*, Vol. 39, No. 6, 1991, pp. 859–861.

[49] K. Miyata: A 12 GHz-band planar waveguide array antenna for compact range application – A preliminary study, *IEEE Transactions on Antennas and Propagation*, Vol. 44, No. 4, 1996, pp. 588–589.

[50] R. C. Johnson, H. A. Ecker, R. A. Moore: Compact range techniques and measurements, *IEEE Transactions on Antennas and Propagation*, Vol. 17, No. 5, 1969, pp. 568–576.

[51] J. R. Descardeci: *The Enlargement and Measurement of the Quiet Zone of a Compact Antenna Test Range*, Doctoral Thesis, Queen Mary & Westfield College, University of London, 1996, 242 p.

[52] A. D. Olver: Compact antenna test ranges, *Proceedings of the Seventh International conference on Antennas and Propagation (ICAP)*, York, UK, 1991, pp. 99–108.

[53] V. J. Vokurka: Seeing double improves indoor range, *Microwave & RF*, February 1985, pp. 71–76, 94.

[54] J. R. Descardeci, C. G. Parini: Dual reflector feed system for a compact antenna test range, *Proceedings of the IEE 9th International Conference on Antennas and Propagation*, Eindhoven, The Netherlands, 1995, pp. 141–144.

[55] M. Philippakis, C. G. Parini: Diffraction effects of a tape covering the gaps of a panelled 'compact range' operating at millimetre waves, *IEE Proceedings*, Vol. 141, Pt. H, No. 2, 1994, pp. 114–122.

[56] A. A. Saleeb: *Theory and Design of Lens-type Compact Antenna Ranges*, Doctoral Thesis, Queen Mary & Westfield College, University of London, 1982, 279 p.

[57] A. D. Olver, A. A. Saleeb: Lens-type compact antenna range, *Electronics Letters*, Vol. 15, No. 14, 1979, pp. 409–410.

[58] T. Hirvonen, J. Tuovinen, A. Räisänen: Lens-type compact antenna test range at mm-waves, *Proceedings of the 21st European Microwave Conference*, Stuttgart, Germany, 1991, pp. 1079–1083.

[59] W. Menzel, B. Huder: Compact range for millimetre-wave frequencies using a dielectric lens, *Electronics Letters*, Vol. 20, No. 19, 1984, pp. 768–769.

[60] A. Vasara, J. Turunen, A. Friberg: Realization of nondiffracting beams with computer-generated holograms, *Journal of Optical Society of America A*, Vol. 6, 1989, pp. 1748–1754.

[61] W.-H. Lee: Computer-generated holograms: techniques and applications, *Progress in Optics XVI*, E. Wolf (ed.), North-Holland, 1978, pp. 121–231.

[62] T. Hirvonen, J. Tuovinen, A. V. Räisänen: Tolerance analysis of a 500 GHz amplitude hologram, *Proceedings of the 6$^{th}$ International Symposium on Space Terahertz Technology*, Pasadena, CA, 1995, pp. 397–406.

[63] R. C. Johnson, H. A. Ecker, J. S. Hollis: Determination of far-field antenna patterns from near-field measurements, *Proceedigns of the IEEE*, Vol. 61, No. 12, 1973, pp. 1668–1694.

[64] L. S. Taylor: The phase retrieval problem, *IEEE Transactions on Antennas and Propagation*, Vol. 29, No. 2, 1981, pp. 386–391.

[65] R. G. Yaccarino, Y. Rahmat-Samii: Phaseless bi-polar planar near-field measurements and diagnostics of array antennas, *IEEE Transactions on Antennas and Propagation*, Vol. 47, No. 3, 1999, pp. 574–583.

[66] G. Junkin, T. Huang, J. C. Bennett: Holographic testing of terahertz antennas, *IEEE Transactions on Antennas and Propagation*, Vol. 48, No. 3, 2000, pp. 409–417.

[67] T. Isernia, G. Leone, R. Pierri: New approach to antenna testing from near field phaseless data: the cylindrical scanning, *IEE Proceedings*, Vol. 139, Pt. H, No. 4, 1992, pp. 363–368.

[68] T. Isernia, G. Leone, R. Pierri: Radiation pattern evaluation from near-field intensities on planes, *IEEE Transactions on Antennas and Propagation*, Vol. 44, No. 5, 1996, pp. 701–710.

[69] A. P. Anderson, G. Junkin, J. E. McCormack: Near-field far-field predictions from single-intensity-planar-scan phase retrieval, *Electronics Letters*, Vol. 25, No. 8, 1989, pp. 519–520.

[70] A. Taflove (ed.): *Computational Electrodynamics: The Finite-Difference Time-Domain Method*, Artech House, Norwood, MA, 1995, 599 p.

[71] K. S. Kunz, R. J. Luebbers: *The Finite Difference Time Domain Method for Electromagnetics*, CRC Press, Boca Raton, 1993, 448 p.

[72] K. S. Yee: Numerical solution of initial boundary value problems involving Maxwell's equations in isotropic media, *IEEE Transactions on Antennas and Propagation*, Vol. 14, No. 3, 1966, pp. 302–307.

[73] J.-P. Berenger: A perfectly matched layer for the absorption of electromagnetic waves, *Journal of Computational Physics*, Vol. 114, 1994, pp. 185–200.

[74] C. M. Furse, S. P. Mathur, O. P. Gandhi: Improvements to the finite-difference time-domain method for calculating the radar cross section of a perfectly conducting target, *IEEE Transactions on Microwave Theory and Techniques*, Vol. 38, No. 7, 1990, pp. 919–927.

[75] C. M. Furse, D. H. Roper, D. N. Buechler, D. A. Christensen, C. H. Durney: The problem and treatment of DC offsets in FDTD simulations, *IEEE Transactions on Antennas and Propagation*, Vol. 48, No. 8, 2000, pp. 1198–1201.

[76] A. C. Cangellaris, R. Lee: On the accuracy of numerical wave simulations based on finite methods, *Journal of Electromagnetic Waves and Applications*, Vol. 6, No. 12, 1992, pp. 1635–1653.

[77] I.S. Kim, W. J. R. Hoefer: Numerical dispersion characteristics and stability factor for the TD-FD method, *Electronics Letters*, Vol. 26, No. 7, 1990, pp. 485–487.

[78] R. C. Booton: *Computational Methods for Electromagnetics and Microwaves*, John Wiley & Sons, New York, 1992, 182 p.

[79] S. D. Gedney, F. Lansing: Explicit time-domain solution of Maxwell's equations using nonorthogonal and unstructured grids, Chapter 11 in *Computational Electrodynamics: The Finite-Difference Time-Domain Method*, A. Taflove (ed.), Artech House, Norwood, MA, 1995, pp. 343–396.

[80] B. Engquist, A. Majda: Absorbing boundary conditions for the numerical simulation of waves, *Mathematics of Computation*, Vol. 31, 1977, pp. 629-651.

[81] G. Mur: Absorbing boundary conditions for the finite-difference approximation of the time-domain electromagnetic-field equations, *IEEE Transactions on Electromagnetic Compatibility*, Vol. 23, 1981, pp. 377-382.

[82] P. A. Tirkas, C. A. Balanis and R. A. Renaut: Higher order absorbing boundary conditions for the finite-difference time-domain method, *IEEE Transactions on Antennas and Propagation*, Vol. 40, 1992, pp. 1215-1222.

[83] K. K. Mei, J. Fang: Superabsorption - a method to improve absorbing boundary conditions, *IEEE Transactions on Antennas and Propagation*, Vol. 40, 1992, pp. 1001-1010.

[84] Z. Wu, J. Fang: Numerical Implementation and performance of perfectly matched layer boundary condition for waveguide structures, *IEEE Transactions on Microwave Theory and Techniques*, Vol. 43, No. 12, 1995, pp. 2676–2683.

[85] A. Taflove, M. E. Brodwin: Numerical solution of steady-state electromagnetic scattering problems using the time-dependent Maxwell's equations, *IEEE Transactions on Microwave Theory and Techniques*, Vol. 23, 1975, pp. 623–630.

[86] A. P. Zhao, A. V. Räisänen, S. R. Cvetkovic: A fast and efficient FDTD algorithm for the analysis of planar microstrip discontinuities by using a simple source excitation scheme, *IEEE Microwave and Guided Wave Letters*, Vol. 5, No. 10, 1995, pp. 341–343.

[87] J. A. Kong: *Electromagnetic Wave Theory*, John Wiley & Sons, New York, 1986, 696 p.

[88] W. L. Stutzman, G. A. Thiele: *Antenna Theory and Design*, John Wiley & Sons, New York, 1981, 598 p.

[89] C. C. Chen: Transmission through a conducting screen perforated periodically with apertures, *IEEE Transactions on Microwave Theory and Techniques*, Vol. 18, No. 9, 1970, pp. 627–632.

[90] J. J. H. Wang: *Generalized Moment Methods in Electromagnetics; Formulation and Computer Solution of Integral Equations*, John Wiley & Sons, New York, 1991, 553 p.

[91] T. M. Hirvonen: *Quasioptical Methods for Antenna Measurements*, Doctoral Thesis, Helsinki University of Technology, 1997, 131 p.

[92] T. Sehm: *Development of Low-profile Radio Link Antennas for Millimeter Waves*, Doctoral Thesis, Helsinki University of Technology, 2000, 92 p.